SCIENCE CHINA
Information Sciences

• RESEARCH PAPER •

October 2020, Vol. 63 202304:1–202304:22
https://doi.org/10.1007/s11432-020-2853-9

Synthesis-free directional modulation for retrodirective frequency diverse array

Sheng KE, Jianping AN* & Shuai WANG

School of Information and Electronics, Beijing Institute of Technology, Beijing 100081*, China*

Received 13 February 2020/Accepted 25 March 2020/Published online 16 September 2020

Abstract Combination of directional modulation (DM) and frequency diverse array (FDA) provides a novel opportunity for enabling physical layer security because of the enhanced ability of distance resolution. However, in the existing studies, the time-varying nature of the FDA pattern is usually ignored. In this paper, a modified model of FDA-DM is proposed, in which the ignored time factor in the previous studies is taken into consideration for providing a new and more accurate perspective on evaluating the security of FDA-DM. Furthermore, we reveal that FDA-DM can achieve angle-dependent and directional-time-coupled-dependent security. After that, based on the retrodirective FDA (RFDA) with a new structure, a novel synthesis-free FDA-DM scheme is proposed for both overcoming the limitations of the FDA-DM scheme and allowing self-tracking the position of the pilot signal without any prior knowledge. Meanwhile, a new set of nonlinear frequency offsets, defined as rearranged linear frequency offsets (RLFOs), is also proposed for both combining the advantages of the linear/nonlinear frequency offsets and bringing conveniences to practical implementation. In addition, the closed-form expression of the average signal-to-artificial-noise-ratio (SANR) is given out for evaluating the security performance of the proposed scheme. Finally, numerical results are presented to verify both the accuracy of the proposed theoretical analysis and the superiority of the RFDA-DM scheme.

Keywords secure transmission, frequency diverse array (FDA), frequency offsets (FOs), retrodirective array, average SANR distribution

Citation Ke S, An J P, Wang S. Synthesis-free directional modulation for retrodirective frequency diverse array. Sci China Inf Sci, 2020, 63(10): 202304, https://doi.org/10.1007/s11432-020-2853-9

1 Introduction

Directional modulation (DM) [1–14], as a keyless physical-layer security transmitting technique with great potentials in wireless communications [15–17], has drawn a wide attention in the past decade. Compared with the secure beamforming techniques, where both the directions of the desired user and the eavesdropper are required in advance, DM can obtain secure transmission relying only on the prior knowledge of the desired user. In the existing studies, DM was usually realized at the radio frequency (RF) front end. For example, in [7], DM was implemented by adjusting the element weights of the phased-array (PA). It was also the first time that a phased-array was used to realize DM. Before that, DM was achieved using the parasitic array [8]. Meanwhile, antenna subset modulation [9], which is designed based on RF switches, may also be categorized as a DM technique owing to its essence of introducing extra points in the constellation along any undesired direction.

Despite all this, the above-mentioned studies are of high computational complexity, making the implementation of DM at the RF side be of low flexibility owing to the characteristic of the RF devices. To

* Corresponding author (email: an@bit.edu.cn)

address this issue, in 2014, a vector approach was proposed for finding the excitation vectors of DM [6], in which the authors pointed out that the essence of DM was capable of both adding artificial noise orthogonal to the steering vector along the desired direction at the transmitter side and updating it at the symbol rate. Meanwhile, the authors in [6] gave out a low-complexity and easy-to-realize method for achieving DM at the baseband. After that, robust designs of DM were implemented in [10, 11], where the authors took the estimation error of the desired direction into consideration. In addition, other typical DM related studies include: a DM transmitter was also designed in [12] for enabling multiple-user communications following the orthogonal vector approach. In [5], the authors used non-uniform linear arrays to realize DM. In [14], the authors discussed the power allocation problem used in the full-duplex unmanned aerial vehicle communication system that is also based on DM.

Besides DM, the impact of artificial noise has also been widely investigated in multi-input multi-output (MIMO) systems in the presence of the eavesdroppers, including performance analysis [18], power allocation [19], and applications in variant scenarios [20–23]. However, all these studies assumed the direction (or the approximate direction) of the desired user was known in advance. When the legitimate direction was unknown or changed, the performance of these systems would degrade dramatically owing to the excellent confidentiality of DM. Thus, these transmitters require re-synthesis and suffer from a heavy computation burden. Unlike the previous studies, the authors in [13] proposed a synthesis-free DM transmitter based on the retrodirective array, in which the transmitter could achieve DM characteristic without relying on the prior knowledge of the user's direction (but at the expense of an extra uplink pilot signal transmitted from the user). This transmitter is capable of supporting multi-users and multi-paths scenarios, although in these scenarios the receiving signal along the desire direction will also be contaminated. Furthermore, the authors derived the perfect DM conditions that the transmitter can send signals without introducing any distortion to all the users in multipath scenarios.

In summary, all the traditional phased-array-based DM techniques have a common limitation, i.e., they depend only on direction. If in-happen both the legitimate receiver and the eavesdroppers can be covered by the same directional beam, the communication becomes no more secure. Recently, frequency diverse array (FDA) has been introduced in DM techniques for offering an extra range-dependent security, in which a small frequency increment is added to each element of the FDA. Because these frequency offsets (FOs)[1)] make the beampatterns range-dependent [24], the system's secure performance can be improved. In fact, before the physical layer security area gets noticed, FDA has already been widely employed in radar for enabling target localization [25–31] and range-dependent beamforming synthesis [32–34]. Most of these techniques are based on linear frequency offsets (LFOs). However, in [35], by combining the DM technique with FDA with symmetrical linear frequency offsets, the authors pointed out the importance of non-linear frequency offsets (NLFOs) in reducing the signal-to-noise-ratio (SNR) at undesired locations. Later in [36, 37], the authors achieved FDA-DM using random frequency offsets (RFOs). In addition, the authors in [38] proposed the FDA-DM techniques using time-modulated logarithmically increasing frequency offsets (LogFOs).

Admittedly, all of the above technologies rely on the prior knowledge of the desired user. Once the location of legitimate users changes, these existing solutions must be re-synthesized with the help of a large amount of calculations. Apart from this limitation, another important concern comes from the fact that most of the FDA-DM related studies [35–41] claim their capability of obtaining point-to-point secure transmission, implying that the transmitted symbols could only be recovered at the desired position. However, it is still impossible to achieve keyless position-dependent secure transmission in the most commonly used "far-field point-to-point LOS channel" model[2)], because electromagnetic waves carrying data always propagate in straight line in free space (i.e., it definitely does not appear only at

1) We use the acronym "FO" to represent frequency offset, while "FOs" is the plural form of FO.

2) From our understanding, 'point-to-point' is slightly different from 'position-dependent'. The former concept requires that the transmitting array and the receiving array can be regarded as two points in the interested angle-range domain, while the latter concept only has such a requirement for the receiving array. Thus, the former concept is stricter than the latter one. Keyless position-dependent secure transmission can still be achieved under non-point-to-point and NLOS scenarios, such as the near-field scenario [42], or using multiple transmitters [43], or in multipath scenarios.

a certain location). The reasons for these studies came to get an unreasonable conclusion are either that the security performance of the FDA was only studied in the angle-range domain at a certain time [35–37], or that the eavesdroppers were not properly synchronized [39, 41], or even the transmission delay was ignored [38, 40]. Despite that, the FDA transmitter can still achieve directional-dependent and range-time-coupled-dependent secure transmission. From this aspect, it still outperforms the phased-array (PA)-based transmitter, which can only achieve directional-dependent secure transmission. The confusing features of the FDA will be elaborated on in the preliminary.

To overcome the limitations in the existing FDA-DM researches, we propose a novel retrodirective FDA (RFDA)-based synthesis-free artificial-noise-aided secure transmission scheme. The main contributions of our work are summarized as follows:

- The model of FDA-based DM is modified by both taking the time factors that are ignored in previous related studies [35–41] into consideration and giving a more explicit interpretation of FDA-based DM. To the best of our knowledge, it is pointed out for the first time that the FDA-DM scheme still causes great troubles for the eavesdroppers along the desired direction with synchronization even though the security in the range dimension cannot be guaranteed. Relying on this new model, which can be regarded as a supplementary work of the previous literatures [35–41], we can give a more accurate description of the security provided by FDA-DM.

- A novel synthesis-free directional modulation technique based on RFDA, which utilizes the self-tracking characteristic of the retrodirective array and overcomes the limitations of the FDA-DM scheme, is proposed. The structure of the proposed RFDA is different from the existing one. Furthermore, it is the first time (to the best of our knowledge) to propose an analog/digital hybrid structure.

- A novel set of frequency offsets defined as rearranged linear frequency offsets (RLFOs) is proposed by combining the advantages of LFOs and other NLFOs. Equipped with RLFOs, the proposed RFDA-DM scheme can achieve angle-range focusing capability as what NLFOs can do, making it be un-achievable when LFOs are used. On the other hand, compared to the other NLFOs, the synthesis-free RFDA-DM transmitter equipped with RLFOs is much easier to implement.

- The closed-form expression of the average signal-to-artificial-noise ratio (SANR) is given out for calculating both the error probability and the achievable rate of the receivers. Moreover, based on Taylor expansion, the main lobe of SANR distribution around the desired location can be described analytically, revealing the fact that the proposed RLFOs and other NLFOs have the similar security performance. Meanwhile, the angle-range ambiguity of LFOs can be explicitly explained in our analytical work, while in some previous FDA-DM researches this limitation is only qualitatively discussed.

The rest of the paper is organized as follows: in Section 2, the system model of FDA is given out, where the directional-dependent and range-time-coupled-dependent characteristics of the FDA are discussed from the beam pattern aspect and the received baseband signal aspect respectively. After that, the modified principle of synthesis-required FDA-DM technique is introduced. In Section 3, we propose the synthesis-free RFDA-DM transmitter and the definition of RLFOs. Furthermore, in Section 4, the average SANR distribution is analyzed, followed by discussing the advantages of RLFOs over other NLFOs in implementation in Section 5. Simulations results are given in Section 6. Finally, conclusion is drawn in Section 7.

Notations. Throughout this paper, boldface lowercase letters are used to denote vectors, boldface capital letters denote matrices. $[\boldsymbol{A}]_{i,j}$ or a_{ij} represents the element at the ith row and the jth column of matrix $\boldsymbol{A}$, and $[\boldsymbol{a}]_i$ or a_i represents the ith element of the vector $\boldsymbol{a}$. $\boldsymbol{0}_N$ and $\boldsymbol{1}_N$ represent N-elements vectors with all elements to be 0 or 1. $\boldsymbol{I}_N$ is an N-dimensional unit array. $\lfloor a \rfloor$ represents the largest integer which is no greater than a. $a(t) * b(t)$ represents the convolution of $a(t)$ and $b(t)$. $(\cdot)^*$, $(\cdot)^{\mathrm{T}}$ and $(\cdot)^{\dagger}$ denote conjugate operator, transpose operator and conjugate transpose operator, respectively. The symbol $\|\cdot\|$ is the norm of a vector and $\mathrm{E}\{\cdot\}$ represents taking expectation of random variables. A symbol $a(t)$ is used to represent a time-continuous signal, while $a[m]$ is a time-discrete signal.

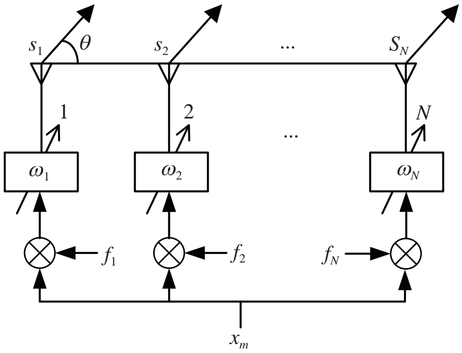

Figure 1 The model of FDA.

2 The preliminary

2.1 The time-variant range-dependent beampattern of FDA

In this paper, we mainly focus on an N-element uniform-linear-FDA (UL-FDA) with equal spacing d, as illustrated in Figure 1. Note that similar discussion can readily be extended to the other array structures. Compared with the conventional phased array, an FDA adds a small frequency offset Δf_l to the lth element. Because all the sub-frequencies are far smaller than the carrier wave frequency f_c, the transmitting frequency at the lth element is $f_l = f_c + \Delta f_l$. Therefore, the spacing d between two adjacent elements should not beyond $\lambda_{\min}/2$ in order to avoid multiple mainlobes from 0 to π, where $\lambda_{\min}$ represents the wavelength corresponding to the largest frequency. The transmitted signal from the l-th element of FDA at the time interval t can be expressed as

$$s_l(t) = x_m \omega_l \mathrm{e}^{\mathrm{j}2\pi(f_c+\Delta f_l)t}, \tag{1}$$

where x_m denotes the m-th transmitted symbol satisfying $|x_m| = 1$, and ω_l is the beamforming coefficient.

To focus on the characteristics of both FDA and DM, we may take a widely employed assumption, i.e., to ignore the environment noise and the path fading effects [6, 13, 38, 41]. With the first element of the transmitting array as the origin of a polar system, the electric field intensity distribution, or in another equivalent way, the received signal of a far-field single-antenna receiver located at (R, θ) at the time interval t can be expressed as

$$\begin{aligned} r(R,\theta,t) &= \sum_{l=1}^{N} s_l\left(t - \frac{R_l}{c}\right) = \sum_{l=1}^{N} x_{\lfloor m-\frac{R}{cT_s}\rfloor} \omega_l \mathrm{e}^{\mathrm{j}2\pi(f_c+\Delta f_l)(t-\frac{R_l}{c})} \\ &= x_{\lfloor m-\frac{R}{cT_s}\rfloor} \mathrm{e}^{\mathrm{j}2\pi f_c\left(t-\frac{R}{c}\right)} \underbrace{\begin{bmatrix} \mathrm{e}^{-\mathrm{j}2\pi\left(f_c\frac{0d\cos\theta}{c}+\Delta f_1\left(t-\frac{R}{c}\right)\right)} \\ \mathrm{e}^{-\mathrm{j}2\pi\left(f_c\frac{1d\cos\theta}{c}+\Delta f_2\left(t-\frac{R}{c}\right)\right)} \\ \vdots \\ \mathrm{e}^{-\mathrm{j}2\pi\left(f_c\frac{(N-1)d\cos\theta}{c}+\Delta f_N\left(t-\frac{R}{c}\right)\right)} \end{bmatrix}^{\dagger}}_{a^{\dagger}(R,\theta,t)} \underbrace{\begin{bmatrix} \omega_1 \\ \omega_2 \\ \vdots \\ \omega_N \end{bmatrix}}_{\omega}, \end{aligned} \tag{2}$$

where $R_l = R - (l-1)d\cos\theta$ denotes the distance between the l-th transmitting antenna and the receiving antenna, c represents the speed of light, and $\boldsymbol{a}^{\dagger}(R,\theta,t)$ stands for the steering vector (SV) of FDA that is angle-range dependent and time-variant. Furthermore, T_s is the symbol period, and the items $\Delta f_l(ld\cos\theta)/c$ is omitted owing to the fact that $\Delta f_l \ll f_l$.

According to the definition, the beam pattern of FDA can be calculated from the module of equation (2), as given by

$$P_{\mathrm{FDA}}(R,\theta,t) = |r(R,\theta,t)|^2 = \left|\boldsymbol{a}^{\dagger}(R,\theta,t)\omega\right|^2. \tag{3}$$

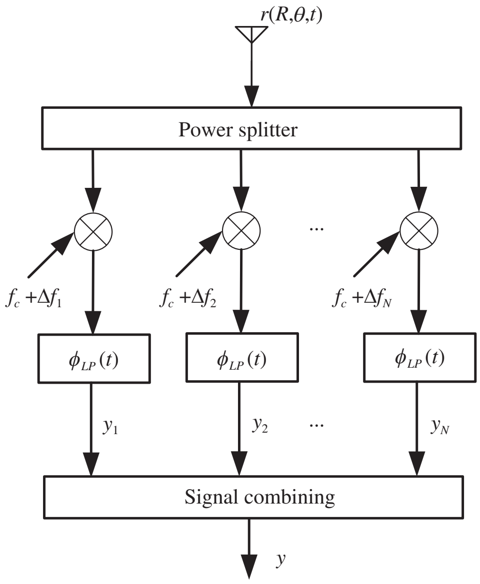

Figure 2 Single-antenna multiple-channel receiver structure.

Therefore, FDA can generate angle-range-dependent beam patterns, and attracts researchers to use this feature of the FDA to achieve point-to-point secure transmission [35–41]. However, most of them are derived only at a specific time, e.g., $t = 0$. As long as the beam pattern of the FDA is time-variant, it is unreasonable to study the security performance of the FDA in only the angle-range domain and at a certain time point. In fact, according to (2), the time factor and the range factor are coupled together, in which case the signal transmitted at time t will arrive at (R_1, θ) at time $t + R_1/c$ while arrive at (R_2, θ) at $t + R_2/c$, implying that the eavesdroppers along the desired direction can also recover the confidential information by correctly calibrating the propagation delay. Unfortunately, because this limitation comes from the physical nature of electromagnetic waves propagating in a wireless environment, it cannot be overcome.

To explain it more explicitly, we temporarily adopt the signal-antenna multiple-channel (SAMC) receiver structure [39] to deal with the received signal, whose structure is shown in Figure 2. Without loss of generality, we assume that all the receivers know all the frequencies (but the receivers may suffer from clock differences from the transmitter). In the following, when we mention synchronization, it represents only time synchronization. Unlike (6) in [39], where the subcarriers are not properly synchronized, the instantaneous output of the l-th channel at time t should be

$$\begin{aligned} y_l &= \left[r(R,\theta,t) \mathrm{e}^{-\mathrm{j}2\pi(f_c+\Delta f_l)\left(t-\frac{R}{c}\right)} \right] * \varphi_{\mathrm{LP}}(t) \\ &= x_{\lfloor m-\frac{R}{cT_S} \rfloor} \mathrm{e}^{\mathrm{j}2\pi f_c \frac{(l-1)d\cos\theta}{c}} = \omega_l x_{\lfloor m-\frac{R}{cT_S} \rfloor} \left[\boldsymbol{a}^{\dagger}(0,\theta,0) \right]_l \omega_l, \end{aligned} \tag{4}$$

where $\varphi_{\mathrm{LP}}(t)$ denotes the impulse response of an ideal low-pass filter. We define zero-phase-time (ZPT) as the moment when the phase of each subcarrier is identical to zero. Furthermore, Eq. (4) implies that with proper synchronization, the ZPT at the receiver should be R/c. It is shown that the received baseband signal with proper synchronization only depends on direction θ, which is different from the beam pattern aspect and no more range-time dependent. Evidently, we must take the impact of time into consideration when discussing the confidentiality performance of the FDA. In addition, it is easy to verify that if the ZPT at the receiver is $R/c + \tau$, i.e., the transmitter and the receiver are not correctly synchronized, the baseband signal of the lth channel should be revised as $y_l(\tau) = x_{\lfloor m-\frac{R}{cT_s} \rfloor} \mathrm{e}^{\mathrm{j}2\pi f_c \tau} [\boldsymbol{a}^{\dagger}(0,\theta,\tau)]_l \omega_l$.

In summary, from the beampattern aspect, the FDA can realize angle-dependent and range-time-dependent beamforming. However, from the aspect of the receiving signal at the receiver side, all the receivers along the desired direction are capable of recovering the information with proper synchronization. In fact, the authors in [44, 45] were also aware of the FDA's problem in achieving point-to-point secure transmission. However, compared to the phased array, whose beam pattern can be calculated from $P_{PA}(\theta) = P_{FDA}(0, \theta, 0)$ and only depends on the angle, FDA can provide not only directional-dependent security but also range-time-coupled-dependent security. This characteristic makes it more difficult for eavesdroppers to recover confidential information from the signal, especially when it is equipped with DM. We may explain it as follows: (1) the first reason is that the eavesdroppers need to know all the exact sub-frequencies. (2) The second one comes from the fact that the eavesdroppers along the desired direction have to be properly synchronized with the transmitter, which is hard to address in the proposed system. (3) The last reason is that, as FDA requires wider bandwidth, the transmitting signal of the FDA has lower power spectral density than PA, making it more difficult to be detected by any unintended receivers in a noisy environment. Consequently, we still assume that the FDA outperforms PA in terms of security performance.

2.2 The modified principle of FDA-based directional modulation

In this subsection, we review the principle of FDA-DM that was proposed in [35, 36, 38] and take the ignored time factor into consideration. We are going to offer our readers a more accurate description of FDA-DM so as to get a deeper understanding of RFDA-based DM (which will be introduced in Section 3). There exists several schemes to realize DM, including genetic algorithm [7] and particle swarm optimization [46]. Among them, the most practical scheme is the vector approach proposed in [6], whose essence is to generate artificial noises orthogonal to the SV corresponding to the channel between the transmitter and the legitimate user.

Compared to the beamforming techniques [47–51], the two main advantages of DM reside in the fact that DM can achieve secure transmission even without the knowledge of the eavesdroppers, as well as that DM can also provide security in high SNR scenarios. The key idea of DM is to distort the constellation points along undesired directions. For this reason, the transmitting weighting vector $\boldsymbol{\omega}$ is required to be updated at the symbol rate, denoted by $\boldsymbol{\omega}_m$, to offer randomicity at other undesired locations. With the prior knowledge of the legitimate user's location (R_u, θ_u), the FDA-DM weighting vector $\boldsymbol{\omega}_m$ can be generated and updated as

$$\boldsymbol{\omega}_m = \frac{\boldsymbol{a}_u}{\|\boldsymbol{a}_u\|_2^2} + \boldsymbol{A}_{\boldsymbol{a}_u}\boldsymbol{\mu}_m, \tag{5}$$

where $\boldsymbol{a}_u$ is assumed to be short for $\boldsymbol{a}(0, \theta_u, 0)$, and $\boldsymbol{A}_{\boldsymbol{a}_u} \in \mathbb{C}^{N\times(N-1)}$ is the unit orthogonal basis of $\mathcal{N}\{\boldsymbol{a}_u^\dagger\}$. Furthermore, $\boldsymbol{\mu}_m$ is updated at the symbol rate and consists of $N-1$ i.i.d. circularly-symmetric complex Gaussian random variables with zero means and variance σ_{AN}^2. Following (4), in the FDA-based DM system, the m-th recovered constellation points of a properly synchronized receiver at (R, θ) can be express as

$$y_m \triangleq \sum_{l=1}^{N} y_{m,l} = x_m\boldsymbol{a}^\dagger(0,\theta,0)\boldsymbol{\omega}_m = \underbrace{x_m\boldsymbol{a}^\dagger(0,\theta,0)\frac{\boldsymbol{a}_u}{\|\boldsymbol{a}_u\|_2^2}}_{\text{desired component}} + \underbrace{x_m\boldsymbol{a}^\dagger(0,\theta,0)\boldsymbol{A}_{\boldsymbol{a}_u}\boldsymbol{\mu}_m}_{\text{artificial noise}}. \tag{6}$$

When $\theta = \theta_u$, we have $\boldsymbol{a}^\dagger(0,\theta_u,0)\frac{\boldsymbol{a}_u}{\|\boldsymbol{a}_u\|_2^2} = 1$, while $\boldsymbol{a}^\dagger(0,\theta,0)\boldsymbol{A}_{\boldsymbol{a}_u} = \mathbf{0}_{N-1}$. Thus the received baseband signal along the desired direction contains only the desired component, enabling the constellation points to be recovered. This characteristic is exactly the same as a PA-DM system. However, when the receiver is not properly synchronized, e.g., the ZPT at the receiver is $R/c+\tau$, the received baseband signal from an FDA-DM transmitter is

$$y_m(\tau) = x_m\mathrm{e}^{\mathrm{j}2\pi f_c\tau}\boldsymbol{a}^\dagger(0,\theta,\tau)\frac{\boldsymbol{a}_u}{\|\boldsymbol{a}_u\|_2^2} + x_m\mathrm{e}^{\mathrm{j}2\pi f_c\tau}\boldsymbol{a}^\dagger(0,\theta,\tau)\boldsymbol{A}_{\boldsymbol{a}_u}\boldsymbol{\mu}_m. \tag{7}$$

Eq. (7) shows that the recovered constellation points of an unsynchronized receiver in the FDA-DM system (even if it is along the desired direction) not only suffer from amplitude attenuation because the module of $\mathrm{e}^{\mathrm{j}2\pi f_c\tau}\boldsymbol{a}^\dagger(0,\theta_u,\tau)\frac{\boldsymbol{a}_u}{\|\boldsymbol{a}_u\|_2^2}$ is always less than 1, but are also contaminated by the non-zero artificial noise $\boldsymbol{a}^\dagger(0,\theta,\tau)\boldsymbol{A}_{\boldsymbol{a}_u}$. On the contrary, in the PA-DM system, owing to the steering vector of PA is time-invariant, the received baseband signal of an unsynchronized receiver is

$$y_{m,PA}(\tau) = x_m \mathrm{e}^{\mathrm{j}2\pi f_c \tau}\boldsymbol{a}^\dagger(0,\theta,0)\frac{\boldsymbol{a}_u}{\|\boldsymbol{a}_u\|_2^2} + x_m \mathrm{e}^{\mathrm{j}2\pi f_c \tau}\boldsymbol{a}^\dagger(0,\theta,0)\boldsymbol{A}_{\boldsymbol{a}_u}\boldsymbol{\mu}_m = x_m \mathrm{e}^{\mathrm{j}2\pi f_c \tau}. \tag{8}$$

Therefore, all the receivers along the desired direction can recover the constellation points with a rotation coefficient, constituting the reason that FDA-DM can still offer better secure performance than PA-DM in the distance dimension.

Let us look into this characteristic from the beampattern aspect and explain the observation that synchronization is more difficult in the FDA-DM system. At time t, according to (2), the FDA-DM transmitter begins to transmit the m-th symbol. The electric field intensity distribution of the FDA-DM system at the same time can be expresses as

$$r(R,\theta,t) = x_{\lfloor m-\frac{R}{cT_s}\rfloor}\mathrm{e}^{\mathrm{j}2\pi f_c\left(t-\frac{R}{c}\right)}\boldsymbol{a}^\dagger(R,\theta,t)\frac{\boldsymbol{a}_u}{\|\boldsymbol{a}_u\|_2^2} + x_{\lfloor m-\frac{R}{cT_s}\rfloor}\mathrm{e}^{\mathrm{j}2\pi f_c\left(t-\frac{R}{c}\right)}\boldsymbol{a}^\dagger(R,\theta,t)\boldsymbol{A}_{\boldsymbol{a}_u}\boldsymbol{\mu}_{\lfloor m-\frac{R}{cT_s}\rfloor}. \tag{9}$$

The average instantaneous SANR at (R,θ), where the average is taken with respect to multiple realizations of $\boldsymbol{\mu}_m$, can be given by

$$\mathrm{SANR}(t;R,\theta) = \frac{\frac{|\boldsymbol{a}^\dagger(R,\theta,t)\boldsymbol{a}_u|^2}{\|\boldsymbol{a}_u\|_2^4}}{\mathrm{E}\{|\boldsymbol{a}^\dagger(R,\theta,t)\boldsymbol{A}_{\boldsymbol{a}_u}\boldsymbol{\mu}_m|^2\}} = \frac{|\boldsymbol{a}^\dagger(R,\theta,t)\boldsymbol{a}_u|^2}{N^2\sigma_{AN}^2\boldsymbol{a}^\dagger(R,\theta,t)\boldsymbol{A}_{a_u}\boldsymbol{A}_{a_u}^\dagger\boldsymbol{a}(R,\theta,t)}. \tag{10}$$

If $\boldsymbol{a}(R,\theta,t)$ is not periodic, i.e., $\boldsymbol{a}(R,\theta,t_1)\neq\boldsymbol{a}(R,\theta,t_2)$, $\forall t_1\neq t_2$, SANR is less than infinity even if $\theta=\theta_u$ when $t\neq R/c$. Considering an extreme case when σ_{AN}^2 goes to infinity, SANR goes to 0 when $t\neq R/c$. This means that the receiver needs to complete synchronization at low-SNR conditions, as known to be a difficult task [52, 53]. However, for PA-DM, the instantaneous SANR along the desired direction is always infinite, requiring no confidentiality to be provided in range dimension.

Apart from that, it is obvious that $\boldsymbol{a}(R,\theta,t)=\boldsymbol{a}(0,\theta,t-\frac{R}{c})$, implying the range factor and the time factor are coupled together (so as to obtain the FDA-DM instantaneous SANR distribution). That is why FDA-DM can provide only range-time-coupled-dependent security but not range-focusing security mentioned in the existing studies.

2.3 The frequency offsets selection

Because the SANR distribution of FDA-DM is dependent on Δf_l, it is very important to take FOs selection into account when designing the FDA-DM transmitters. Generally speaking, the frequency offsets can be categorized into two classes, i.e., LFOs and NLFOs. For the former, the subcarriers' frequencies are set as

$$f_l = f_c + (l-1)\Delta f, \quad \forall l = 1,2,\ldots,N, \tag{11}$$

where the subcarriers' frequencies follow a linear function with respect to the corresponding antenna index. Evidently, LFOs have an identical frequency interval Δf. For those FOs that do not satisfy this definition, they are classified as NLFOs. Among them, two special cases are most commonly used, namely, the LogFOs [33] and the RFOs [36, 54]. Some related studies are still based on LFOs [24, 26, 55], but in other references [27, 33, 54], the authors have noticed that the FDA-DM transmitters with NLFOs can be employed for solving the directional-range ambiguity problem caused by LFOs, which will also be analyzed from the SANR distribution aspect later in this research.

3 The synthesis-free directional modulation technique based on retrodirective FDA

The above-mentioned principle of the FDA-DM has three disadvantages: first, it requires prior knowledge of the location of the legitimate user. Second, when the user's position changes, the unit orthogonal basis

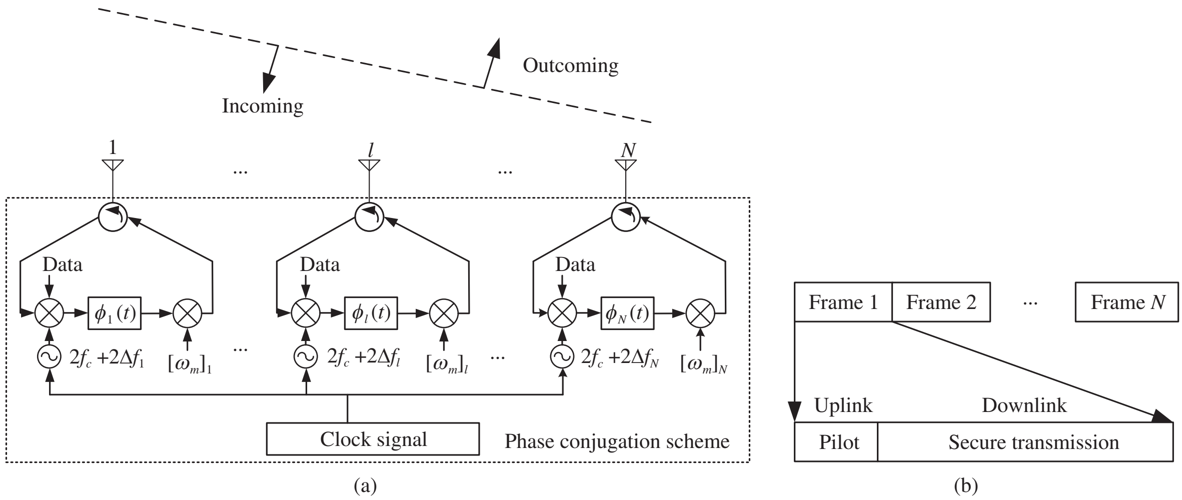

Figure 3 Illustrations of: (a) retrodirective FDA-DM scheme based on Pon's structure; (b) the time slots of RFDA-DM.

of $\boldsymbol{a}_u$ is required to be resynthesized, thus demanding a heavy computational cost. Last but not least, the range-time-dependent confidentiality provided by FDA-DM causes troubles not only for eavesdroppers, but also for the legitimate user with synchronization.

To address the limitations in the synthesis-required FDA-DM, we propose a novel synthesis-free DM technique based on RFDA, as well as a new set of NLFOs named as RLFOs. Before introducing RFDA-DM scheme, let us first give a brief introduction of retrodirective array, which can offer self-tracking by re-radiating the phase-conjugated incoming signal without any prior knowledge of the direction of the legitimate user. The reason why a phase-conjugating retrodirective (RDA) can offer self-tracking functionality is the reciprocity between the uplink channel and the downlink channel, while the principle of the phase-conjugation at the same frequency can be demonstrated by the trigonometric equivalence of the product of two cosine functions, i.e. [56],

$$v_{\mathrm{RD}} = V_{\mathrm{RF}} \cos\left(2\pi f_{\mathrm{RF}} t + \phi\right) V_{\mathrm{LO}} \cos\left(2\pi f_{\mathrm{LO}} t\right), \tag{12}$$

where V_{RF} and V_{LO} denote the input and local oscillator signal amplitudes with the frequency f_{RF} and f_{LO}, respectively. If $f_{\mathrm{LO}} = 2f_{\mathrm{RF}}$, owing to the fact that there are no negative frequency in realistic, with an ideal lowpass filter to remove the component at $3f_{\mathrm{RF}}$, the phase-conjugation of the incoming signal is completed. RDA in such a structure can be categorized into the Pon's structure [57].

3.1 Synthesis-free RFDA-DM technique

In order to introduce the self-tracking functionality to FDA, we proposed a novel RFDA based on the Pon's structure, whose principle is illustrated in Figure 3(a). The proposed structure, which is different from the existing ones [41, 58, 59], requires the incoming signal to contain multi-tones and an ideal bandpass filter to be added to each element of the array (i.e., to remove all the undesired frequencies). This structure is only for the convenience of our following discussion, as the bandpass filters may be difficult to realize in practical systems. The realization problem will be discussed later after introducing RLFOs.

Unlike FDA-DA, RFDA-DM requires fully-synchronized (but not properly synchronized) clocks in the base station (BS) and the legitimate user; i.e., the ZPTs of the base station and the legitimate user are both 0. The fully-synchronized clocks can be obtained from a satellite navigation system like GPS and BeiDou. We assume that all the eavesdroppers keep silent to prevent exposure. Similar to other literatures based on RFDA, each RFDA-DM frame consists of two stages in our proposed scheme (see Figure 3(b)), while in the first stage, the desired user transmits the pilots to the BS, and in the second stage, the BS transmits confidential information to the desired user. In each frame, the position of the legitimate user relative to the base station does not change. To be more specific, in the first time slot, the uplink signal from the legitimated user is designed as[3)]

$$s^{[u]}(t) = \sum_{i=1}^{N} \mathrm{e}^{\mathrm{j}2\pi f_i t}. \tag{13}$$

The incoming signal at the l-th element of RFDA can be expresses as

$$r_l^{[u]}(t) = \sum_{i=1}^{N} \mathrm{e}^{\mathrm{j}2\pi f_i \left(t - \frac{R_u-(l-1)d\cos\theta_u}{c}\right)}. \tag{14}$$

In the l-th channel, the incoming signal is mixed with an LO signal with the frequency $f_{LO,l} = 2f_l$. In the second time slot, after a composition of operations, including mixing with the local frequencies, removing undesired components via the ideal bandpass filter and being weighted by the DM coefficient $[\boldsymbol{\omega}_m]_l$, the downlink transmitted signal of the l-th element, which also carries the secret information, can be expressed as

$$\begin{aligned} s_l^{[d]}(t) &= x_m \left[\boldsymbol{\omega}_m\right]_l \left\{ \left[r_l^{[u]}(t)\mathrm{e}^{-\mathrm{j}2\pi f_{LO,l}t} \right] * \phi_l(t) \right\} \\ &= x_m \left[\boldsymbol{\omega}_m\right]_l \mathrm{e}^{-\mathrm{j}2\pi f_l (t + \frac{R_u-(l-1)d\cos\theta_u}{c})}, \end{aligned} \tag{15}$$

while the DM weighting vectors are generated following the equation:

$$\boldsymbol{\omega}_m = \sqrt{\frac{P}{N}}\mathbf{1}_N + \boldsymbol{A}_1\boldsymbol{\mu}_m, \tag{16}$$

where $A_1 \in \mathbb{C}^{N\times(N-1)}$ is the unit orthogonal basis of $\mathcal{N}\{\mathbf{1}_N^{\mathrm{T}}\}$, and $\boldsymbol{\mu}_m$ follows the definition in (5). Based on (16), the total transmit power of the base station is $P + (N-1)\sigma_{AN}^2$. As the DM weighting vectors are generated independently from $\boldsymbol{a}_u$ or the incoming signals, the DM characteristic is realized without synthesis, i.e., synthesis-free. Consequently, the instantaneous received signal at (R,θ) can be given by

$$\begin{aligned} r^{[d]}(R,\theta,t) &= \sum_{l=1}^{N} s_l\left(t - \frac{R-(l-1)d\cos\theta}{c}\right) \\ &= x_{\lfloor m-\frac{R}{cT_s}\rfloor} \sum_{l=1}^{N} \left[\boldsymbol{\omega}_{\lfloor m-\frac{R}{cT_s}\rfloor}\right]_l \mathrm{e}^{-\mathrm{j}2\pi f_l \left(t + \frac{(R_u-R)-(l-1)d[\cos\theta_u-\cos\theta]}{c}\right)}. \end{aligned} \tag{17}$$

Utilizing the SAMC structure illustrated in Figure 2 to demodulate the downlink signal, replacing the subscript $\lfloor m - R/cT_s\rfloor$ with $\hat{m}$, and assuming the ZPT of the receiver is τ, the $\hat{m}$-th recovered symbol is given by [4)]

$$\begin{aligned} y_{\hat{m}}^{[d]}(\tau) &= \sum_{l=1}^{N} \left\{ \left[r^{[d]}(R,\theta,t)\mathrm{e}^{\mathrm{j}2\pi f_l(t-\tau)} \right] * \varphi_{\mathrm{LP}}(t) \right\} = x_{\hat{m}} \sum_{l=1}^{N} [\omega_{\hat{m}}]_l \, \mathrm{e}^{-\mathrm{j}2\pi f_l (\frac{(R_u-R)-(l-1)d[\cos\theta_u-\cos\theta]}{c}+\tau)} \\ &= \sqrt{\frac{P}{N}} x_{\hat{m}} \mathrm{e}^{-\mathrm{j}2\pi f_c (\frac{R_u-R}{c}+\tau)} \boldsymbol{a}^{\dagger}\left(R-R_u, \arccos\left[\cos\theta-\cos\theta_u\right], -\tau\right)\mathbf{1}_N \\ &\quad + x_{\hat{m}} \mathrm{e}^{-\mathrm{j}2\pi f_c (\frac{R_u-R}{c}+\tau)} \boldsymbol{a}^{\dagger}\left(R-R_u, \arccos\left[\cos\theta-\cos\theta_u\right], -\tau\right)\boldsymbol{A}_1\boldsymbol{\mu}_{\hat{m}}. \end{aligned} \tag{18}$$

Obviously, $\boldsymbol{a}\left(R_u - R, \arccos\left[\cos\theta_u - \cos\theta\right], 0\right) = \mathbf{1}_N$, if $(R,u) = (R_u,\theta_u)$. Therefore, the legitimate user, whose ZPT is 0, can receive the original and uncontaminated constellations. Moreover, it can be easily proved that $\boldsymbol{a}\left(R_u - R, \arccos\left[\cos\theta_u - \cos\theta\right], 0\right) = \mathbf{1}_N$ if and only if (iff.) $(R,u) = (R_u,\theta_u)$ for NLFOs. So in a RFDA-DM system equipped with NLFOs, the self-tracking angle-range focusing

3) We use the superscript "[u]" to represent signals used in uplink communications and to distinguish the signals from those used in downlink communications, which are labeled by the superscript "[d]".

4) When $z < -1$ or $z > 1$, the arccosine function is given as $\arccos(z) = -i\log[z + i(1-z^2)^{1/2}]$.

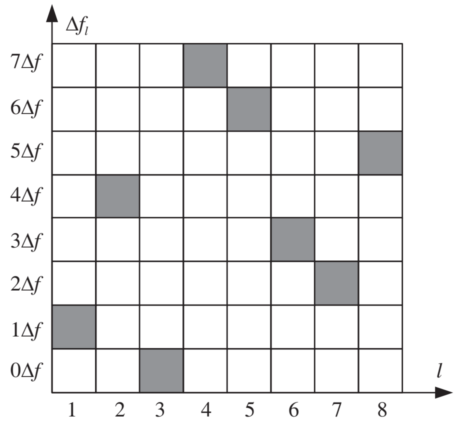

Figure 4 A sketch map of RLFOs with $N = 8$, whose corresponding rearrange matrix $\boldsymbol{P}$ is $[\boldsymbol{e}_2, \boldsymbol{e}_5, \boldsymbol{e}_1, \boldsymbol{e}_8, \boldsymbol{e}_7, \boldsymbol{e}_4, \boldsymbol{e}_3, \boldsymbol{e}_6]$.

characteristic is realized, and any undesired receivers with fully-synchronized clock will suffer from the AN.

We must emphasize that the above discussion is based on the fully-synchronized clocks in the base station and all the receivers. In fact, the eavesdroppers along the desired direction can still recover the symbols with proper phase calibration; i.e., the ZPT of the eavesdropper at (R, θ_u) should be $(R - R_u)/c$, which is different from the FDA-DM scheme. However, as we have pointed out, owing to the existence of AN, such a proper synchronization still remains a difficult task for the eavesdroppers along the desired direction in an RFDA-DM system. On the contrary, the legitimate user does not need any phase calibration process as long as the clock is fully synchronized.

Apart from that, another concern is about timing accuracy. If there is a timing error between the base station and the legitimate user, this timing error will be doubled by adopting our scheme when the downlink signal reaches the UE again. However, because the error cannot be too large, e.g., the timing error of the GPS navigation system can be less than 10 ns [60], the difficulty of synchronization at the UE can be substantially reduced.

3.2 The rearranged linear frequency offsets

The above-mentioned RFDA-DM scheme is applicable for arbitrary frequency offsets. In this subsection, we propose a novel set of frequency offsets, which is defined as below.

Definition 1 (Rearranged linear frequency offsets)**.** RLFOs are a set of nonlinear frequency offsets, and they can be rearranged to a set of LFOs. In mathematical form, a set of frequency offsets $\Delta\boldsymbol{f} = [\Delta f_1, \ldots, \Delta f_N]^{\mathrm{T}}$ can be called as RLFOs if $\exists \boldsymbol{P} = [\boldsymbol{e}_{l_1}, \boldsymbol{e}_{l_2}, \ldots, \boldsymbol{e}_{l_N}] \neq \boldsymbol{I}$, where $\boldsymbol{e}_i$ is an unit column vector with ith element being 1, $l_i \in \{1, \ldots, N\}$, and $l_i \neq l_j$ if $i \neq j$, $\boldsymbol{P}\Delta\boldsymbol{f}$ is LFOs. $\boldsymbol{P}$ is defined as a rearranging matrix.

Figure 4 gives an example of RLFOs. To the best of our knowledge, it is the first time that the concept of RLFOs is proposed. We would like to remind our readers of distinguishing RLFOs from the random frequency diverse array defined in (1) of [36], where k_n is i.i.d. distributed and does not follow our definition of RLFOs. Obviously, RLFOs are special cases of NLFOs, while the summation of RLFOs is equivalent to that of LFOs. In Section 4, we will see that RLFOs combine the advantages of LFOs and NLFOs, and in most scenarios, RLFOs are the optimal choice.

4 Performance evaluation of RFDA-DM

With the basic knowledge of the synthesis-free RFDA-DM scheme, we now turn to analyze the security performance of the system. In this section, we choose to analyze the average SANR distribution of our scheme. Average SANR distribution is an important measurement to evaluate our system as it is strongly related to security performance. For example, according to the definition of achievable rate [36]

$$R_u = \log(1 + \overline{\mathrm{SANR}}(R_u, \theta_u, 0)), \tag{19}$$

$$R_{e,i} = \log\left(1 + \overline{\mathrm{SANR}}(R_{e,i}, \theta_{e,i}, \tau_{e,i})\right), \tag{20}$$

the secrecy rate of our proposed scheme can be given as

$$R = \min_{i\in\mathcal{J}} \{R_u - R_{e,i}\}, \tag{21}$$

where the ith eavesdropper is located as $(R_{e,i}, \theta_{e,i})$ and its ZPT is $\tau_{e,i}$. R_u represents the achievable rate at the legitimate user, $R_{e,i}$ represents the achievable rate at the ith eavesdropper, and $\mathcal{J}$ represents the set of all the potential eavesdroppers.

Another important measurement related to secure performance is the symbol error rate (SER). Similarly, the SER distribution is also equivalent to the average SANR distribution. Without loss of generality, we assume that μ_m is a complex Gaussian random vector. Consequently, the artificial noise component in (18) can be regarded as an additive white Gaussian noise. According to the formula (6-16) in [61], the SER distribution of a receiver at (R, θ), whose ZPT is τ, can be expressed as

$$P_{\mathrm{S}}(R, \theta, \tau) = 2Q\left(\sqrt{2\overline{\mathrm{SANR}}(R, \theta, \tau)} \sin\frac{\pi}{M}\right), \tag{22}$$

when multiple phase shift keying (MPSK) is used and $Q(\cdot)$ is the right tail distribution function of the standard normal distribution. With the expression of the average SANR distribution, our readers can easily get the secrecy rate and the SER distribution of the proposed scheme.

As the weighting vector of the RFDA-DM scheme is updated at the symbol rate, we try to analyze the average SANR distribution across multiple symbols. Notice in the expression of the downlink recovered baseband symbols given in (18), only $\boldsymbol{\mu}_m$ is the random variable, and thus the expectation is only taken with respect to $\boldsymbol{\mu}_m$. Denoting $\Delta R \triangleq R - R_u$ and $\Delta\theta \triangleq \arccos[\cos\theta_u - \cos\theta]$, we can get the expression of the average SANR as

$$\begin{aligned}\overline{\mathrm{SANR}}(R, \theta, \tau) &= \frac{P\boldsymbol{a}^\dagger(\Delta R, \Delta\theta, -\tau)\mathbf{1}_N\mathbf{1}_N^\dagger\boldsymbol{a}(\Delta R, \Delta\theta, -\tau)}{N\boldsymbol{a}^\dagger(\Delta R, \Delta\theta, -\tau)\boldsymbol{A}_1\mathrm{E}\{\boldsymbol{\mu}_m\boldsymbol{\mu}_m^\dagger\}\boldsymbol{A}_1^\dagger\boldsymbol{a}(\Delta R, \Delta\theta, -\tau)} \\ &= \frac{P\boldsymbol{a}^\dagger(\Delta R, \Delta\theta, -\tau)\mathbf{1}_N\mathbf{1}_N^\dagger\boldsymbol{a}(\Delta R, \Delta\theta, -\tau)}{N\sigma_{AN}^2\boldsymbol{a}^\dagger(\Delta R, \Delta\theta, -\tau)\boldsymbol{A}_1\boldsymbol{A}_1^\dagger\boldsymbol{a}(\Delta R, \Delta\theta, -\tau)}.\end{aligned} \tag{23}$$

We would like to point out that when discussing the performance in a noisy environment, we only need to add the noise power to the denominator of the average SANR distribution. Before further simplifying the above expression, we have to give an useful lemma first.

Lemma 1. For $\forall N \geqslant 2$ and $\forall \boldsymbol{A}_1$ given in (16), $\exists \boldsymbol{U}$ which is an $N-1$ dimensional orthogonal matrix, satisfies $\boldsymbol{A}_1 = \overline{\boldsymbol{A}}_1\boldsymbol{U}$, where $\overline{\boldsymbol{A}}_1 \in \mathbb{R}^{N\times(N-1)}$ is also an unit orthogonal basis of $\mathbf{1}_N$, and satisfies

$$\left[\overline{\boldsymbol{A}}_1\overline{\boldsymbol{A}}_1^{\mathrm{T}}\right]_{ij} = \begin{cases} \dfrac{N-1}{N}, & i = j, \\ -\dfrac{1}{N}, & i \neq j. \end{cases} \tag{24}$$

Proof. Such an $\overline{\boldsymbol{A}}_1$ is given as

$$\overline{\boldsymbol{A}}_1 = \begin{bmatrix} -\sqrt{\dfrac{1}{N}} & -\sqrt{\dfrac{1}{N}} & \cdots & -\sqrt{\dfrac{1}{N}} \\ \dfrac{N-1+\sqrt{N}}{N+\sqrt{N}} & -\dfrac{1}{N+\sqrt{N}} & \cdots & -\dfrac{1}{N+\sqrt{N}} \\ -\dfrac{1}{N+\sqrt{N}} & \dfrac{N-1+\sqrt{N}}{N+\sqrt{N}} & \cdots & -\dfrac{1}{N+\sqrt{N}} \\ \vdots & \vdots & \ddots & \vdots \\ -\dfrac{1}{N+\sqrt{N}} & -\dfrac{1}{N+\sqrt{N}} & \cdots & \dfrac{N-1+\sqrt{N}}{N+\sqrt{N}} \end{bmatrix} \in \mathbb{R}^{N\times(N-1)}. \tag{25}$$

With that, it can be verified straightforwardly that $\overline{\boldsymbol{A}}_1$ forms an unit orthogonal basis of the null space of $\mathbf{1}_N$, and satisfies (24), and thus the second part of lemma is proved.

For the first part of the lemma, as we have already known that $\overline{\boldsymbol{A}}_1$ is an unit orthogonal basis of the null space of $\mathbf{1}_N$, and then any other unit orthogonal basis of $\mathbf{1}_N$, denoted as $\boldsymbol{A}_1$, also lies in the subspace spanned by $\overline{\boldsymbol{A}}_1$. So every $\boldsymbol{A}_1$ can be expressed by $\overline{\boldsymbol{A}}_1$ via a linear transformation defined by $\boldsymbol{U}$, i.e., $\boldsymbol{A}_1 = \overline{\boldsymbol{A}}_1\boldsymbol{U}$.

Based on Lemma 1, we can use the exact matrix $\overline{\boldsymbol{A}}_1$ to get some tractable results. These results derived from $\overline{\boldsymbol{A}}_1$ are also correct for other $\boldsymbol{A}_1$. To explain that, any $\boldsymbol{\omega}_m$ generated via other $\boldsymbol{A}_1$ can be re-written as $\mathbf{1}_N + \overline{\boldsymbol{A}}_1\boldsymbol{U}\boldsymbol{\mu}_m$, and $\boldsymbol{U}\boldsymbol{\mu}_m$ can be regarded as a new random variable $\overline{\boldsymbol{\mu}}_m \backsim \mathcal{CN}(\mathbf{0}_{N-1}, \sigma_{AN}^2\boldsymbol{I}_{N-1})$, which satisfies the same probability distribution of $\boldsymbol{\mu}_m$.

Firstly, Eq. (23) can be transformed to (28), where from (26) to (27), we separate the summations in the numerator and denominator into two parts: the first part contains the components where $l_1 = l_2$, and the residual components are included in the second part. And Eqs. (27) and (28) are based on Lemma 1. Eq. (28) is the closed-form expression of the average SANR distribution in the RFDA-DM system. From (28), we can see that the received average SANR is directional-dependent and range-time-coupled-dependent.

$$\overline{\mathrm{SANR}}(\Delta R,\Delta\theta,\tau) = \frac{P\sum_{l_1=1}^{N}\sum_{l_2=1}^{N}\mathrm{e}^{\mathrm{j}2\pi(f_c\frac{(l_1-l_2)d\cos\Delta\theta}{c}-(\Delta f_{l_1}-\Delta f_{l_2})(\frac{\Delta R}{c}-\tau))}}{N\sigma_{AN}^2\sum_{l_1=1}^{N}\sum_{l_2=1}^{N}[\overline{\boldsymbol{A}}_1\overline{\boldsymbol{A}}_1^{\mathrm{T}}]_{l_1,l_2}\mathrm{e}^{\mathrm{j}2\pi(f_c\frac{(l_1-l_2)d\cos\Delta\theta}{c}-(\Delta f_{l_1}-\Delta f_{l_2})(\frac{\Delta R}{c}-\tau))}} \tag{26}$$

$$= \frac{PN + 2P\mathcal{R}\{\sum_{l_1=1}^{N-1}\sum_{l_2=l_1+1}^{N}\mathrm{e}^{\mathrm{j}2\pi(f_c\frac{(l_1-l_2)d\cos\Delta\theta}{c}-(\Delta f_{l_1}-\Delta f_{l_2})(\frac{\Delta R}{c}-\tau))}\}}{N(N-1)\sigma_{AN}^2 + 2N\sigma_{AN}^2\mathcal{R}\{\sum_{l_1=1}^{N-1}\sum_{l_2=l_1+1}^{N}[\overline{\boldsymbol{A}}_1\overline{\boldsymbol{A}}_1^{\mathrm{T}}]_{l_1,l_2}\mathrm{e}^{\mathrm{j}2\pi(f_c\frac{(l_1-l_2)d\cos\Delta\theta}{c}-(\Delta f_{l_1}-\Delta f_{l_2})(\frac{\Delta R}{c}-\tau))}\}} \tag{27}$$

$$= \frac{PN + 2P\sum_{l_1=1}^{N-1}\sum_{l_2=l_1+1}^{N}\cos[2\pi(f_c\frac{(l_1-l_2)d\cos\Delta\theta}{c} - (\Delta f_{l_1}-\Delta f_{l_2})(\frac{\Delta R}{c}-\tau))]}{N(N-1)\sigma_{AN}^2 - 2\sigma_{AN}^2\sum_{l_1=1}^{N-1}\sum_{l_2=l_1+1}^{N}\cos[2\pi(f_c\frac{(l_1-l_2)d\cos\Delta\theta}{c} - (\Delta f_{l_1}-\Delta f_{l_2})(\frac{\Delta R}{c}-\tau))]}. \tag{28}$$

Next, let us focus on the scenario when all the receivers are equipped with fully-synchronized clocks, i.e., $\tau = 0$, to get some more meaningful results. Utilizing the second-order Taylor expansion to approximate the cosine function around $(\Delta R, \cos\Delta\theta) = (0, 0)$, the average SANR distribution around the desired location can be approximately expressed as

$$\overline{\mathrm{SANR}}_{\mathrm{main}}(\Delta R,\Delta\theta,0) \approx \frac{PN^2 - 4P\pi^2\sum_{l_1=1}^{N-1}\sum_{l_2=l_1+1}^{N}(a_{l_1,l_2}\cos\Delta\theta - b_{l_1,l_2}\Delta R)^2}{4\pi^2\sigma_{AN}^2\sum_{l_1=1}^{N-1}\sum_{l_2=l_1+1}^{N}(a_{l_1,l_2}\cos\Delta\theta - b_{l_1,l_2}\Delta R)^2}, \tag{29}$$

where

$$a_{l_1,l_2} = f_c\frac{(l_1-l_2)d}{c}, \quad b_{l_1,l_2} = \frac{\Delta f_{l_1} - \Delta f_{l_2}}{c}. \tag{30}$$

Then the contour lines around the desired location can be derived. Let $\overline{\mathrm{SANR}}_{\mathrm{main}}$ equals to C, which may represent the minimal SANR requirement when a receiver can work normally, Eq. (29) can be transformed into a quadratic form, denoted as

$$\boldsymbol{z}^{\mathrm{T}}\boldsymbol{B}\boldsymbol{z} = \frac{PN^2}{4\pi^2(P + C\sigma_{AN}^2)}, \tag{31}$$

where

$$\boldsymbol{z} = \begin{bmatrix}\cos\Delta\theta\\ \Delta R\end{bmatrix}, \quad \boldsymbol{B} = \sum_{l_2=l_1+1}^{N}\sum_{l_1=1}^{N-1}\begin{bmatrix}a_{l_1,l_2}^2 & -a_{l_1,l_2}b_{l_1,l_2}\\ -a_{l_1,l_2}b_{l_1,l_2} & b_{l_1,l_2}^2\end{bmatrix}. \tag{32}$$

Denote

$$\boldsymbol{\alpha} \triangleq [a_{1,2}, a_{1,3}, \ldots, a_{1,N}, a_{2,3}, a_{2,4}, \ldots, a_{N-1,N}]^{\mathrm{T}}, \tag{33}$$

$$\boldsymbol{\beta} \triangleq [b_{1,2}, b_{1,3}, \ldots, b_{1,N}, b_{2,3}, b_{2,4}, \ldots, b_{N-1,N}]^{\mathrm{T}}. \tag{34}$$

Then, the eigenpolynomial of the matrix $\boldsymbol{B}$ is

$$\lambda^2 - (\boldsymbol{\alpha}^{\mathrm{T}}\boldsymbol{\alpha} + \boldsymbol{\beta}^{\mathrm{T}}\boldsymbol{\beta})\lambda + \|\boldsymbol{\alpha}\|^2\|\boldsymbol{\beta}\|^2 - (\boldsymbol{\alpha}^{\mathrm{T}}\boldsymbol{\beta})^2 = 0. \tag{35}$$

The characteristics of the quadratic form (31) are summerized in the following theorem.

Theorem 1. For NLFOs, $\boldsymbol{B}$ is a positive-definite matrix. For LFOs, $\boldsymbol{B}$ is a rank-1 positive-semidefinite matrix.

Proof. According to the Cauchy-Schwartz inequality,

$$\|\boldsymbol{\alpha}\|^2\|\boldsymbol{\beta}\|^2 - (\boldsymbol{\alpha}^{\mathrm{T}}\boldsymbol{\beta})^2 \geqslant 0, \tag{36}$$

where the equality holds iff. $\boldsymbol{\alpha}$ and $\boldsymbol{\beta}$ are linearly dependent. That is equivalent to $\Delta f_l = l\Delta f$, i.e., LFOs are utilized. In this scenario, utilizing the Vieta's formulas, the two eigenvalues of $\boldsymbol{B}$ are $\lambda_1 = 0, \lambda_2 = \boldsymbol{\alpha}^{\mathrm{T}}\boldsymbol{\alpha} + \boldsymbol{\beta}^{\mathrm{T}}\boldsymbol{\beta} > 0$. So rank$(\boldsymbol{B}) = 1$ and $\boldsymbol{B}$ is positive-semidefinite.

On the other hand, for NLFOs, we have $\lambda_1 + \lambda_2 = \boldsymbol{\alpha}^{\mathrm{T}}\boldsymbol{\alpha} + \boldsymbol{\beta}^{\mathrm{T}}\boldsymbol{\beta} > 0, \lambda_1\lambda_2 = \|\boldsymbol{\alpha}\|^2\|\boldsymbol{\beta}\|^2 - (\boldsymbol{\alpha}^{\mathrm{T}}\boldsymbol{\beta})^2 > 0$. Therefore, $\lambda_1 > 0$ and $\lambda_2 > 0$. So $\boldsymbol{B}$ is positive-definite.

Based on Theorem 1, we can come to the most important conclusion of this part.

Corollary 1. The RFDA-DM transmitter with LFOs has direction-range ambiguity problem. While for NLFOs, the contour line (31) is an ellipse and thus directional-range-dependent secure transmission can be realised.

Proof. For NLFOs, as the matrix $\boldsymbol{B}$ is positive-definite. Therefore, Eq. (31) represents an ellipse. Moreover, when C increases, the right side of (31) will decrease, which means the area of the ellipse will decrease. Extremely, when C goes to infinite, the ellipse will degenerate to a point. Therefore, with NLFOs, the area where the receiver can get high average SANR will be restricted in an elliptical area around the desired location. Therefore, directional-range-dependent secure transmission can be realized.

On the other hand, for LFOs, as $\boldsymbol{B}$ is rank-1 and positive-semidefinite, we can utilize the following eigenvalue decomposition (EVD) of $\boldsymbol{B}$, i.e.,

$$\boldsymbol{B} = \lambda_2 \boldsymbol{p}_2 \boldsymbol{p}_2^{\mathrm{T}}, \tag{37}$$

where $\boldsymbol{p}_2$ represents the eigenvector corresponding to the positive eigenvalue λ_2. Eq. (31) then can be revised as

$$\boldsymbol{p}_2^{\mathrm{T}}\boldsymbol{z} = \pm \underbrace{\sqrt{\frac{PN^2}{4\lambda_2\pi^2(P + C\sigma_{AN}^2)}}}_{\xi}. \tag{38}$$

Eq. (38) represents two seperate lines on the $(\Delta R, \cos\Delta\theta)$ plane. For those $(\Delta R, \cos\Delta\theta)$ which satisfies $-\xi \leqslant \boldsymbol{p}_2^{\mathrm{T}}\boldsymbol{z} \leqslant \xi$, the average SANR is larger than C. Thus, in a linear "belt" zone on the $(\Delta R, \cos\Delta\theta)$ plane, both the legitimate user and the eavesdroppers will have high SANR and can recover the original information.

The authors wish readers to notice that the problem of LFOs is much more severe than the direction-range ambiguity problem. In fact, the above conclusion is based on the fully-synchronized assumption between the base station and all potential receivers. We can see that with LFOs, the infinite signal-to-noise ratio appears in all directions at different distances. That means with proper synchronization, all receivers, regardless of their locations, may recover confidential information. Therefore, FDA equipped with LFOs is not suitable for physical layer security.

At last, as RLFOs are special cases of NLFOs, we can point out that the secure performance of the proposed RFDA-DM scheme with RLFOs is similar to that with NLFOs.

5 The superiorities of RLFOs in implementation

In Section 3, the principle of the synthesis-free RFDA-DM scheme has been proposed. We have pointed out that RLFOs outperform LFOs from the aspect of average SANR distribution. However, the ad-

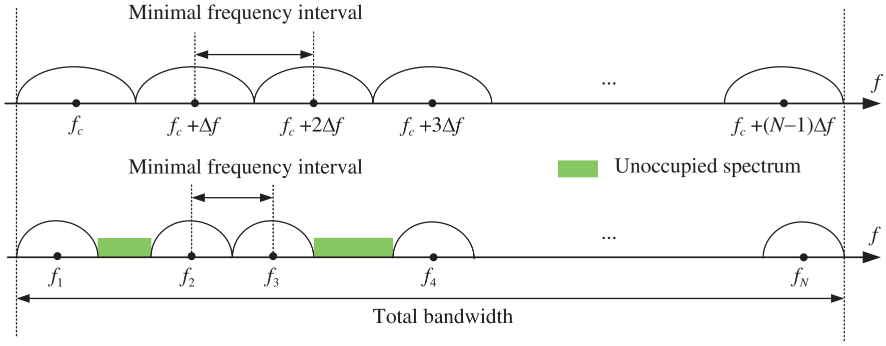

Figure 5 (Color online) The frequency spectrums of RLFOs (above) and other NLFOs (below) with the same total bandwidth.

vantages of RLFOs over other NLFOs are not revealed. In fact, the advantages of RLFOs are mainly reflected in the actual system implementation, which are discussed briefly as below.

(1) When the symbol rate is fixed, the transmitter with RLFOs requires narrower total bandwidth compared with other NLFOs.

Generally, in order to avoid spectrum overlapping, we must have

$$\min_{i,j}\{|\Delta f_i - \Delta f_j|\} \geqslant R_s,\ \forall i \neq j. \tag{39}$$

This is equivalent to

$$B = \max_{i,j}\{\Delta f_i - \Delta f_j\} \geqslant (N-1)R_s, \tag{40}$$

where B is the total bandwidth. The equality holds iff. LFOs or RLFOs are used. Therefore, for other NLFOs, the transmitter requires wider bandwidth than RLFOs. On the other hand, when the total bandwidth is fixed, the transmitter with RLFOs can achieve higher transmission rate than that with other NLFOs. A graphic explanation is given in Figure 5, where for ordinary NLFOs there are unoccupied frequency spacings, and the width of each subband, which is proportional to the symbol rate, is smaller than that of RLFOs.

(2) The RFDA-DM base station with RLFOs is easier to implement than that with other NLFOs.

In Figure 3(a), we give the illustration of RFDA based on Pon's structure, where we add a band-pass filter in each channel to remove those undesired frequencies. However, as $\Delta f_l \ll f_c$, it is very difficult to design such a band-pass filter at RF. An alternative solution is to downconvert the incoming signal to IF or baseband before filtering. The phase conjugation process is also performed at intermediate frequency (IF) or baseband, and then the phase-conjugated signal is re-modulated and upconverted to the ideal frequency again. In fact, this idea has already been proposed in [62], where a retrodirectivity phased array is realized via an analog-digital (A/D) hybrid structure. The A/D hybrid structure not only simplifies the system design, but also provides additional flexibility. For example, RDA based on the Pon's structure can only work in full-duplex mode, which requires high RF isolation. However, the A/D hybrid structure can support both full-duplex communications and half-duplex communications.

By doing so, we can also improve the structure of the base station in our proposed RFDA-DM scheme. Interestingly, we find that a RFDA-DM base-station with RLFOs does not require any filter at baseband as we can utilize the orthogonality between different subcarriers. To be more specific, a prototype of RFDA-DM base station equipped with RLFOs based on A/D hybrid structure is illustrated in Figure 6[5)], where the lowpass filters at IF are used to remove noise outside the effective bandwidth and are of low cost. The ADCs sample at the rate of $f_s = N\Delta f$, where Δf is the minimal frequency interval of the RLFOs. Then after the digital down-conversion cooperated with the direct digital synthesis (DDS) module [63],

5) In Figure 6, ADC is short for analog-to-digital converter, and DAC is short for digital-to-analog converter.

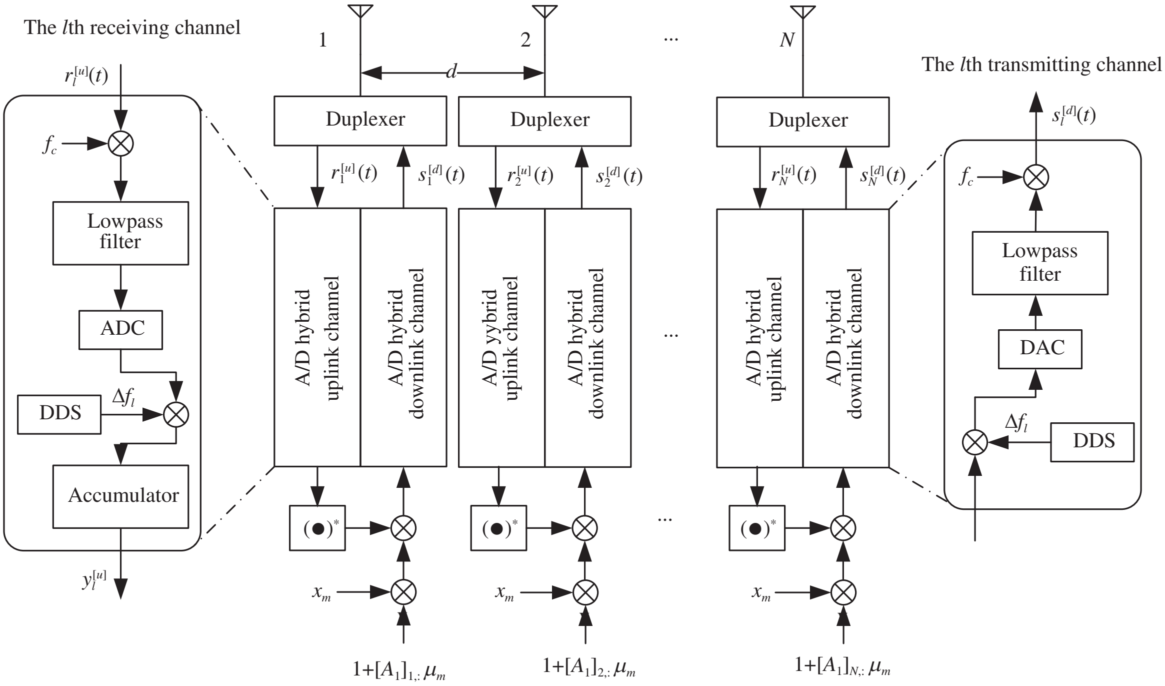

Figure 6 A prototype of RFDA-DM base station equipped with RLFOs, where the phase conjugation is realized at baseband.

the input of the accumulator in the lth uplink channel can be expressed as

$$\begin{aligned} r_l^{[u]}[k] &= \left(r_l^{[u]}(t)\mathrm{e}^{-\mathrm{j}2\pi(f_c+\Delta f_l)t}\right) * \delta\left(t-\frac{k}{f_s}\right) \\ &= \left[\mathrm{e}^{-\mathrm{j}2\pi f_c\frac{R_u}{c}}\sum_{i=1}^{N}\mathrm{e}^{\mathrm{j}2\pi\left(f_c\frac{\iota d\cos\theta_u}{c}-(\Delta f_i-\Delta f_l)\frac{R_u}{c}\right)}\mathrm{e}^{\mathrm{j}2\pi(\Delta f_i-\Delta f_l)t}\right] * \delta\left(t-\frac{k}{f_s}\right) \\ &= \mathrm{e}^{-\mathrm{j}2\pi f_c\frac{R_u}{c}}\sum_{i=1}^{N}\mathrm{e}^{\mathrm{j}2\pi(f_c\frac{ld\cos\theta_u}{c}-(\Delta f_i-\Delta f_l)\frac{R_u}{c})}\mathrm{e}^{\mathrm{j}2\pi(\Delta f_i-\Delta f_l)\frac{k}{f_s}}, \end{aligned} \tag{41}$$

where $\delta(t)$ is the unit-impulse function. Then the accumulator takes the sum of N sampling points, which can be expressed as

$$\begin{aligned} y_l^{[u]} &= \sum_{k=1}^{N} r_l^{[u]}[k] = \mathrm{e}^{-\mathrm{j}2\pi f_c\frac{R_u}{c}}\sum_{i=1}^{N}\mathrm{e}^{\mathrm{j}2\pi(f_c\frac{ld\cos\theta_u}{c}-(\Delta f_i-\Delta f_l)\frac{R_u}{c})}\cdot\sum_{k=1}^{N}\mathrm{e}^{\mathrm{j}2\pi(\Delta f_i-\Delta f_l)\frac{k}{f_s}} \\ &= \mathrm{e}^{-\mathrm{j}2\pi f_c\frac{R_u}{c}}\sum_{i=1}^{N}\mathrm{e}^{\mathrm{j}2\pi(f_c\frac{ld\cos\theta_u}{c}-(\Delta f_i-\Delta f_l)\frac{R_u}{c})}\cdot\sum_{k=1}^{N}\mathrm{e}^{\mathrm{j}2\pi\frac{(n_i-n_l)k}{N}}, \end{aligned} \tag{42}$$

where $\Delta f_i = n_i\Delta f, \Delta f_l = n_l\Delta f$. Notice for RLFOs and LFOs, the following equation holds

$$\sum_{k=1}^{N}\mathrm{e}^{\mathrm{j}2\pi\frac{(n_i-n_l)k}{N}} = \begin{cases} N, & \text{if } n_i = n_{l_k}, \\ 0, & \text{others.} \end{cases} \tag{43}$$

This means that for RLFOs, the accumulator can remove the undesired frequencies. On the other hand, for other NLFOs, Eq. (43) does not hold. So the accumulators in Figure 6 need to be replaced with lowpass filters accordingly, which will increase the hardware complexity.

Another unexpected benefit brought by RLFOs is that, although we only want to obtain the phase-conjugation of the incoming signal, the uplink receiving channel of the A/D hybrid structure illustrated in Figure 6 is actually equivalent to the minimum variance unbiased (MVU) estimator of $N\mathrm{e}^{-\mathrm{j}2\pi f_c\frac{R_u}{c}}\boldsymbol{a}^{\dagger}(R_u,$

$\theta_u, 0)$. To give a short explanation, assume we have N observations $r_l^{[u]}[k]$ of the lth channel, where $k = 1, \ldots, N$, and we know that they satisfy the relationship:

$$\boldsymbol{r}_l = \boldsymbol{D}^\dagger \boldsymbol{a}_l + \boldsymbol{n}_l, \tag{44}$$

where $\boldsymbol{n}_l$ is the Gaussian white noise satisfying $\mathcal{CN}\left(\mathbf{0}_N, \sigma^2 \boldsymbol{I}_N\right)$, and

$$\boldsymbol{r}_l = \begin{bmatrix} r_l^{[u]}[1]\mathrm{e}^{-\mathrm{j}2\pi f_c \frac{1}{f_s}} \\ r_l^{[u]}[2]\mathrm{e}^{-\mathrm{j}2\pi f_c \frac{2}{f_s}} \\ \vdots \\ r_l^{[u]}[N]\mathrm{e}^{-\mathrm{j}2\pi f_c \frac{N}{f_s}} \end{bmatrix}, \quad \boldsymbol{a}_l = \begin{bmatrix} \mathrm{e}^{-\mathrm{j}2\pi f_c \frac{R_u}{c}} \left[\boldsymbol{a}^\dagger\left(R_u, \theta_u, 0\right)\right]_l \\ \mathrm{e}^{-\mathrm{j}2\pi f_c \frac{R_u}{c}} \left[\boldsymbol{a}^\dagger\left(R_u, \theta_u, 0\right)\right]_l \\ \vdots \\ \mathrm{e}^{-\mathrm{j}2\pi f_c \frac{R_u}{c}} \left[\boldsymbol{a}^\dagger\left(R_u, \theta_u, 0\right)\right]_l \end{bmatrix}, \tag{45}$$

$$\boldsymbol{D} = \begin{bmatrix} \mathrm{e}^{-\mathrm{j}2\pi\Delta f_1 \frac{1}{f_s}} & \mathrm{e}^{-\mathrm{j}2\pi\Delta f_1 \frac{2}{f_s}} & \ldots & \mathrm{e}^{-\mathrm{j}2\pi\Delta f_1 \frac{N}{f_s}} \\ \mathrm{e}^{-\mathrm{j}2\pi\Delta f_2 \frac{1}{f_s}} & \mathrm{e}^{-\mathrm{j}2\pi\Delta f_2 \frac{2}{f_s}} & \ldots & \mathrm{e}^{-\mathrm{j}2\pi\Delta f_2 \frac{N}{f_s}} \\ \vdots & \vdots & \ddots & \vdots \\ \mathrm{e}^{-\mathrm{j}2\pi\Delta f_N \frac{1}{f_s}} & \mathrm{e}^{-\mathrm{j}2\pi\Delta f_N \frac{2}{f_s}} & \ldots & \mathrm{e}^{-\mathrm{j}2\pi\Delta f_N \frac{N}{f_s}} \end{bmatrix}. \tag{46}$$

Obviously, for RLFOs, $\boldsymbol{D}$ is an out-of-order Fourier transform matrix for RLFOs and satisfies $\boldsymbol{D}\boldsymbol{D}^\dagger = N\boldsymbol{I}_N$. Consequently, the MVU estimator of $\boldsymbol{a}_l$ is given by [64]

$$\hat{\boldsymbol{a}}_l = (\boldsymbol{D}\boldsymbol{D}^\dagger)^{-1}\boldsymbol{D}\boldsymbol{r}_l = \frac{1}{N}\boldsymbol{D}\boldsymbol{r}_l, \tag{47}$$

where the lth element of $\boldsymbol{D}\boldsymbol{r}_l$ side is equivalent to the expression of $y_l^{[u]}$ given in (42). Therefore, by putting all $y_l^{[u]}$ together, we can get the MVU estimation of $N\mathrm{e}^{-\mathrm{j}2\pi f_c \frac{R_u}{c}} \boldsymbol{a}^\dagger\left(R_u, \theta_u, 0\right)$. As the MVU estimator reaches the Cramer-Rao Lower Bound, we cannot get a more accurate estimation about the uplink channel. Therefore, the performance of the RFDA-DM scheme equipped with RLFOs in noisy environments can be guaranteed.

Besides the above discussion, with RLFOs, observing (13) and (17), the uplink transmitting signal and the downlink received signal at the user side can use the inverse fast Fourier transform/fast Fourier transform (IFFT/FFT) modules to further decrease the hardware cost.

To draw a conclusion to Sections 4 and 5, with RLFOs, the proposed RFDA-DM scheme can restrict the main lobe of the average SANR distribution in an elliptical area around the desired location, which can provide better security performance than LFOs. Moreover, RLFOs have many advantages over other NLFOs and are more suitable for implementation.

6 Simulation results

In this section, we provide several numerical experiments to evaluate the performance of the RFDA-DM scheme. In our simulations, the center frequency is set as $f_c = 10$ GHz and the frequency interval as $\Delta f = 20$ kHz. The rearranging matrix $\boldsymbol{P}$ is randomly selected for each simulation. The legitimate user is located at $(R_u, \theta_u) = (10\ \text{km}, 60^\circ)$. To offer better demonstrations of the range-dependent security performance provided by the FDA, free-space attenuation at different distances is normalized as 1. Moreover, our simulations are performed without environment noise, to give eavesdroppers great chances to recover the confidential information.

Essentially, the security of the FDA-DM scheme is provided by the artificial noise, which is generated from $\boldsymbol{\mu}_m$ given in (5) and (16). However, the base station should spend extra power on the AN. It can be easily predicted that if more power is used to transmit AN, the better security performance of FDA-DM can achieve. Therefore, according to (16), we define the power efficiency (PE) of an FDA-DM transmitter as the ratio between the power used to transmit the information and the total transmit power, i.e.,

$$\mathrm{PE} = \frac{P}{P + (N-1)\sigma_{AN}^2} \times 100\%. \tag{48}$$

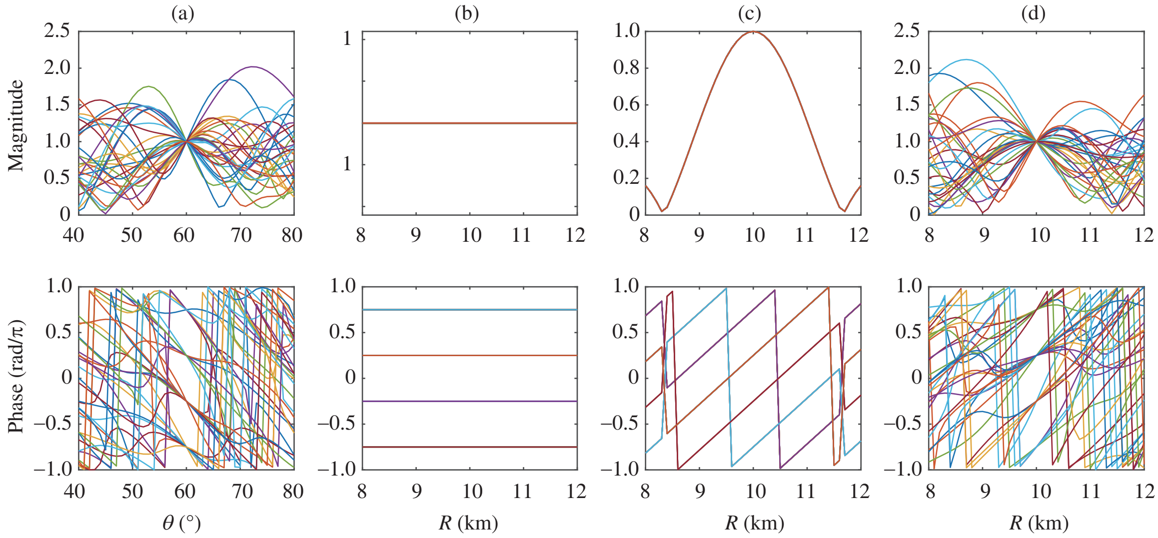

Figure 7 (Color online) The far-field magnitude and phase patterns of (a) FDA-DM and PA-DM w.r.t. θ, and $R = R_u$, (b) PA-DM w.r.t R, and $\theta = \theta_u$, (c) FDA beamforming w.r.t R, and $\theta = \theta_u$, (d) FDA-DM w.r.t R, and $\theta = \theta_u$, where $N = 9$, PE is 50% ((a), (b), (d)) or 100% ((c)).

In our simulations, P is set as 1 W. Obviously, when PE $= 100\%$, no power is used to transmit AN. This situation is therefore equivalent to the traditional beamforming.

The first experiment is to compare the differences among the PA-DM scheme, the FDA beamforming scheme, and the FDA-DM scheme. The simulated magnitude and phase patterns of different schemes with respect to range and angle are given in Figure 7. 30 randomly generated quadrature phase shift keying (QPSK) symbols are plotted in each subplot. To offer more readable graphics and to make a fairer comparison between the legitimate user and the eavesdroppers, the coefficient $\mathrm{e}^{\mathrm{j}2\pi f_c(t-R/c)}$ in (9) has been reasonably compensated as it affects all sub-bands and only causes a rotation of the original constellations but no distortion. The subplots in the first column show that the FDA-DM can obtain directional-dependent security just as PA-DM can do [6]. However, as to the range dimension, the results are given in the rest subplots, we can see that along the desired direction, the PA-DM scheme cannot provide any security. For FDA beamforming, undistorted constellation points can be recovered at the peak of the magnitude, and thus the eavesdroppers along the desired direction can easily complete synchronization through power detection. Moreover, from the phase pattern of the FDA beamforming scheme, we can always see that there are QPSK symbols being transmitted, which means the transmitting signal can be easily detected, especially in high SNR scenarios. In this sense, FDA-DM can provide better security performance than the other two approaches, because at a certain time, the constellation points can only be detected at a certain point in range dimension and the magnitude and the phase patterns at other points are irregular. Therefore, synchronization in the receivers becomes much more difficult than utilizing PA-DM and FDA beamforming. In the meantime, we would like to remind our readers again that this undistorted point will appear at different distances at different times, so the FDA-DM cannot guarantee security in distance but only can provide range-time-coupled-dependent security.

In the second experiment, several simulation results on the 2D symbol-error-rate (SER) distributions of the RLFO-based RFDA-DM scheme are presented. In these simulations, 10^6 QPSK symbols are used at each point. According to (18), the SER of a receiver is dependent on its location (R, θ) and the time difference τ from the base station. Therefore, in order to visualize the simulation results, our experiment is divided into 3 cases: (case1) the SER distribution in the $(\Delta R, \cos\Delta\theta)$ plane with $\tau = 0$, (case2) the SER distribution in the $(\Delta R, \tau)$ plane with $\theta = \theta_u$, and (case3) the SER distribution in the $(\cos\Delta\theta, \tau)$ plane with $R = 8$ km.

Firstly in Figure 8, the 2D SER distribution simulation results of the LFO-RFDA-DM scheme and the RFDA-based beamforming scheme (i.e., PE $= 100\%$) with fully synchronized clocks are presented as

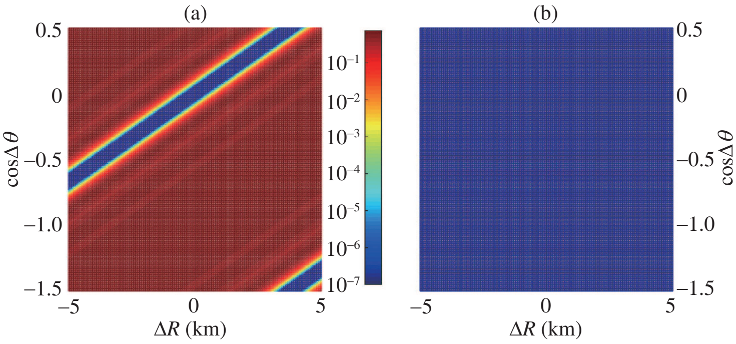

Figure 8 (Color online) The simulated 2-D SER distribution of the RFDA-DM scheme in case1, where $N = 9$ and (a) with LFOs, PE $= 50\%$, (b) with RLFOs, PE $= 100\%$.

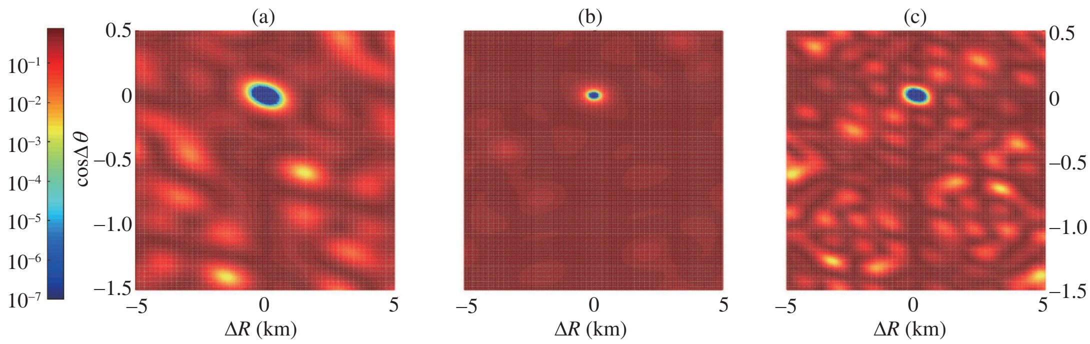

Figure 9 (Color online) The simulated 2-D SER distribution of the RFDA-DM scheme with RLFOs in case1, where (a) $N = 9$, PE $= 50\%$, (b) $N = 9$, PE $= 10\%$, (c) $N = 16$, PE $= 50\%$.

two counterexamples of the proposed RLFO-RFDA-DM scheme. We can see that the LFO-RFDA-DM scheme suffers from the range-angle ambiguity problem and the RFDA-based beamforming scheme even cannot provide any security in the noiseless or high-SNR environment. That means these two schemes are not suitable for secure transmission, especially when the locations of the eavesdroppers are unknown and the SNR is high[6)].

In comparison to the two schemes mentioned above, the 2-D SER distribution simulation results of the proposed RLFO-RFDA-DM scheme are given in Figure 9. From Figure 9(a), we can see that the nulling area of the SNR distribution is restricted around the desired location, which means that angle-range-dependent secure transmission is achieved. Moreover, with the decrease of PE and the increase of N, the nulling zone becomes smaller, which means the scheme can provide better resolution. Our theoretical derivation in Section 4 is also verified from these figures, as the projection of the nulling region to the $(\Delta R, \cos\Delta\theta)$ plane is an ellipse, which is consistent with Corollary 1.

Besides these results, two simulations, which have not been studied in previous literatures as far as we have known, are presented in Figure 10. In these two cases, the effects of the clock difference τ on the zero-SER position are investigated. We assume the ZPTs of the legitimate user and the eavesdroppers are all τ. It can be seen from Figure 10(b) that τ does not affect the security performance in the angular dimension as the zero-SER position only appears when $\cos\Delta\theta = 0$. However, as in this simulation, R is 8 km rather than 10 km, so the zero-SER position is not at $\tau = 0$ but at approximately -6.6 ms, where $(8 - 10)$ km ≈ -6.6 ms$\times c$. On the other hand, it is shown in Figure 10(a) that when τ changes, the zero-SER position also changes in the range dimension. This means that eavesdroppers along the desired direction still can crack the range-dependent security provided by the RFDA-DM scheme with proper synchronization, though it is a very tough task. In addition, we can see that with the fully-synchronized clocks provided by the GPS, the base station can focus the zero-SER position very closed to the desired

6) All the simulation results of SER distribution are presented under logarithmic z-axis, and an impossible SER in these simulations (10^{-7}) is added to avoid negative infinite and to offer a readable color bar.

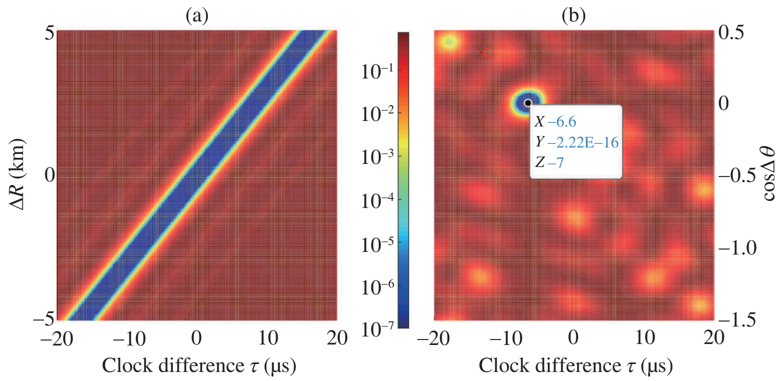

Figure 10 (Color online) The simulated 2-D SER distribution of the RLFO-RFDA-DM scheme in (a) case2 and (b) case3, where $N = 9$, PE = 50%.

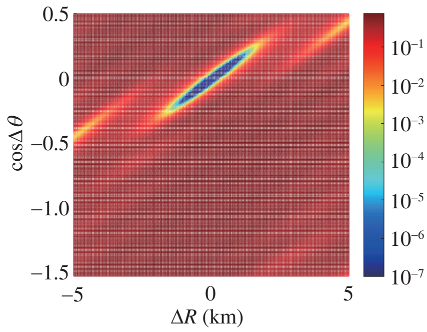

Figure 11 (Color online) The simulated 2-D SER distribution of the RFDA-DM scheme with LogFOs, where $N = 9$, PE = 50%.

position under the given simulation conditions, and thus the retrodirectivity can be guaranteed.

Next, we compare the performance between RLFOs and other NLFOs. As a typical type of NLFOs, LogFOs have been widely adopted in other related studies [33, 38]. LogFOs are defined as

$$\Delta f_l = \Delta f \cdot \log_a l, \quad l = 1, 2, \ldots, N. \tag{49}$$

In order to make a fair comparison, we assume the total bandwidth is fixed. As a result, the frequency interval of NLFOs should be set as $\Delta f_{\mathrm{LogFO}} = \frac{N-1}{\log_a N}\Delta f_{\mathrm{RLFO}}$. In our simulation, a is set as 2 while $\Delta f_{\mathrm{LogFO}}$ is correspondingly set as 7.92 kHz. The simulation result of LogFO-RFDA-DM scheme in case1 is given in Figure 11, where the nulling zone is larger than that of RLFOs with the same PE, N and total bandwidth. This means that the RLFOs cause less information leakage around the desired location than LogFOs.

At last, in order to have a better comparison between the simulation results and the theoretical analysis, the 1-dimensional SER curves along the desired direction and at the desired distance are presented in Figure 12(a) and (b), respectively. Based on (22) and (28), we can derive the theoretical SER curves. Obviously, it also can be seen that in these two figures, the theoretical curves exactly match the numerical results, which verifies the accuracy of our analysis. Moreover, with more transmitting antennas or lower power efficiency, the RFDA-DM scheme will have narrower main lobes and lower sidelobes, and thus better security performance can be achieved. It can also be seen from the figures that the zero-SER position is affected by the timing accuracy, and thus the range-time-coupled-dependent security of the FDA-DM scheme is verified as well.

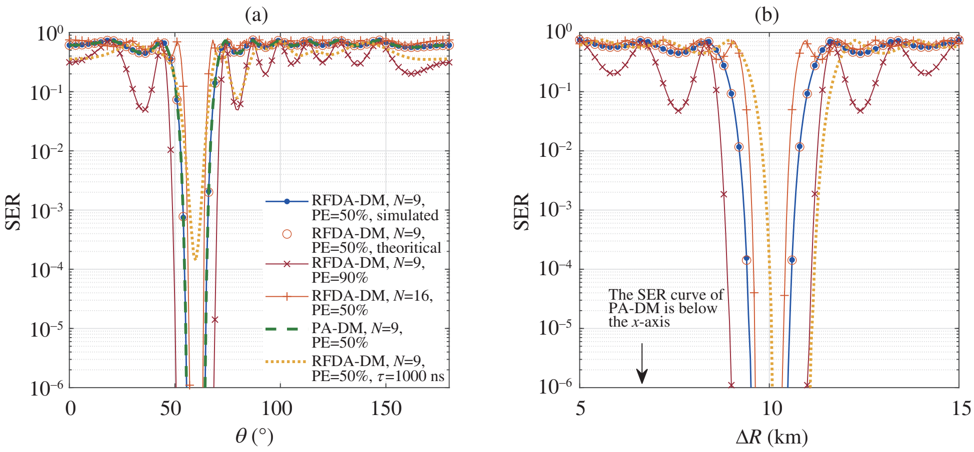

Figure 12 (Color online) The simulated 1-D SER curves of the RLFO-RFDA-DM scheme and the PA-DM scheme with respect to (a) θ with $R = R_u$ and (b) R with $\theta = \theta_u$.

7 Conclusion

In this paper, both the relevant theories and the techniques of directional modulation were improved based on frequency diverse array. First of all, we modified the model of FDA-base DM. It was pointed out that the security over distance provided by FDA-DM is also coupled with time, which provides a more accurate model and a new perspective for researching, even though FDA-DM still outperforms PA-DM. After that, we proposed a synthesis-free DM technique based on the retrodirective FDA with a new structure. The proposed scheme was shown to be capable of overcoming the limitations of FDA-DM, thus allowing the device to self-tracking the legitimate user's position while simultaneously transmitting synthesis-free orthogonal artificial noises so as to increase the difficulties in synchronization for the eavesdroppers. Furthermore, we also proposed a new set of NLFOs, called RLFOs, which can be employed for solving the directional-range ambiguity problem caused by LFOs and bring a lot of convenience to practical implementation. In addition, the closed-form expression of average SANR distribution was given out for evaluating the performance of the proposed scheme. Numerical results show the superiority of the RLFO-RFDA-DM scheme and verify the accuracy of our theoretical work.

Acknowledgements This work was supported in part by National Natural Science Foundation of China (Grant Nos. 61620106001, U1836201).

References

1 Daly M P, Bernhard J T. Beamsteering in pattern reconfigurable arrays using directional modulation. IEEE Trans Antenn Propagat, 2010, 58: 2259–2265
2 Daly M P, Daly E L, Bernhard J T. Demonstration of directional modulation using a phased array. IEEE Trans Antenn Propagat, 2010, 58: 1545–1550
3 Shi H, Alan T. Direction dependent antenna modulation using a two element array. In: Proceedings of the 5th European Conference on Antennas and Propagation (EUCAP), Rome, 2011. 812–815
4 Shi H, Tennant A. Secure physical-layer communication based on directly modulated antenna arrays. In: Proceedings of Loughborough Antennas Propagation Conference (LAPC), Loughborough, 2012. 1–4
5 Liu F, Wang L, Xie J. Directional modulation technique for linear sparse arrays. IEEE Access, 2019, 7: 13230–13240
6 Ding Y, Fusco V F. A vector approach for the analysis and synthesis of directional modulation transmitters. IEEE Trans Antenn Propagat, 2014, 62: 361–370
7 Daly M P, Bernhard J T. Directional modulation technique for phased arrays. IEEE Trans Antenn Propagat, 2009, 57: 2633–2640
8 Babakhani A, Rutledge D B, Hajimiri A. A near-field modulation technique using antenna reflector switching. In: Proceedings of 2008 IEEE International Solid-State Circuits Conference - Digest of Technical Papers, IEEE, 2008. 188–605
9 Valliappan N, Lozano A, Heath R W. Antenna subset modulation for secure millimeter-wave wireless communication. IEEE Trans Commun, 2013, 61: 3231–3245
10 Hu J, Shu F, Li J. Robust synthesis method for secure directional modulation with imperfect direction angle. IEEE Commun Lett, 2016, 20: 1084–1087

11 Shu F, Wu X, Li J, et al. Robust synthesis scheme for secure multi-beam directional modulation in broadcasting systems. IEEE Access, 2016, 4: 6614–6623

12 Ding Y, Fusco V. Orthogonal vector approach for synthesis of multi-beam directional modulation transmitters. Antenn Wirel Propag Lett, 2015, 14: 1330–1333

13 Ding Y, Fusco V. A synthesis-free directional modulation transmitter using retrodirective array. IEEE J Sel Top Signal Process, 2017, 11: 428–441

14 Lu Z, Sun L, Zhang S, et al. Optimal power allocation for secure directional modulation networks with a full-duplex UAV user. Sci China Inf Sci, 2019, 62: 080304

15 Du C, Zhang Z, Wang X, et al. Optimal duplex mode selection for D2D-aided underlaying cellular networks. IEEE Trans Veh Technol, 2020, 69: 3119–3134

16 Luo S X, Zhang Z S, Wang S, et al. Network for hypersonic UCAV swarms. Sci China Inf Sci, 2020, 63: 140311

17 Rong B, Zhang Z, Zhao X, et al. Robust superimposed training designs for MIMO relaying systems under general power constraints. IEEE Access, 2019, 7: 80404–80420

18 Yan S, Yang N, Land I, et al. Three artificial-noise-aided secure transmission schemes in wiretap channels. IEEE Trans Veh Technol, 2018, 67: 3669–3673

19 Shu F, Xu L, Wang J, et al. Artificial-noise-aided secure multicast precoding for directional modulation systems. IEEE Trans Veh Technol, 2018, 67: 6658–6662

20 Goel S, Negi R. Guaranteeing secrecy using artificial noise. IEEE Trans Wirel Commun, 2008, 7: 2180–2189

21 Nguyen N P, Ngo H Q, Duong T Q, et al. Secure massive MIMO with the artificial noise-aided downlink training. IEEE J Sel Areas Commun, 2018, 36: 802–816

22 Wang B, Mu P C, Yang P Z, et al. Two-step transmission with artificial noise for secure wireless SIMO communications. Sci China Inf Sci, 2015, 58: 042308

23 Li B, Fei Z S. Probabilistic-constrained robust secure transmission for energy harvesting over MISO channels. Sci China Inf Sci, 2018, 61: 022303

24 Wang W Q, So H C. Transmit subaperturing for range and angle estimation in frequency diverse array radar. IEEE Trans Signal Process, 2014, 62: 2000–2011

25 Wang W Q. Subarray-based frequency diverse array radar for target range-angle estimation. IEEE Trans Aerosp Electron Syst, 2014, 50: 3057–3067

26 Xu J, Liao G, Zhu S, et al. Joint range and angle estimation using MIMO radar with frequency diverse array. IEEE Trans Signal Process, 2015, 63: 3396–3410

27 Sammartino P F, Baker C J, Griffiths H D. Frequency diverse MIMO techniques for radar. IEEE Trans Aerosp Electron Syst, 2013, 49: 201–222

28 Qin S, Zhang Y D, Amin M G, et al. Frequency diverse coprime arrays with coprime frequency offsets for multitarget localization. IEEE J Sel Top Signal Process, 2017, 11: 321–335

29 Khan W, Qureshi I M, Basit A, et al. Range-bins-based MIMO frequency diverse array radar with logarithmic frequency offset. Antenn Wirel Propag Lett, 2016, 15: 885–888

30 Liao Y, Wang W-Q, Shao H. Symmetrical logarithmic frequency diverse array for target imaging. In: Proceedings of 2018 IEEE Radar Conference (RadarConf18), 2018. 39–42

31 Basit A, Qureshi I M, Khan W, et al. Cognitive frequency diverse array radar with symmetric non-uniform frequency offset. Sci China Inf Sci, 2016, 59: 102314

32 Khan W, Qureshi I M. Frequency diverse array radar with time-dependent frequency offset. Antenn Wirel Propag Lett, 2014, 13: 758–761

33 Khan W, Qureshi I M, Saeed S. Frequency diverse array radar with logarithmically increasing frequency offset. Antenn Wirel Propag Lett, 2015, 14: 499–502

34 Ma Y, Wei P, Zhang H. General focusing beamformer for FDA: mathematical model and resolution analysis. IEEE Trans Antenn Propagat, 2019, 67: 3089–3100

35 Wang W Q. DM using FDA antenna for secure transmission. IET Microwaves Antenn Propagat, 2017, 11: 336–345

36 Hu J, Yan S, Shu F, et al. Artificial-noise-aided secure transmission with directional modulation based on random frequency diverse arrays. IEEE Access, 2017, 5: 1658–1667

37 Wei X, Xiao Y, Xiao Y, et al. Spatial and directional modulation with random frequency diverse array. In: Proceedings of 2018 IEEE 8th Annual Computing and Communication Workshop and Conference (CCWC), 2018. 976–979

38 Cheng Q, Zhu J, Xie T, et al. Time-invariant angle-range dependent directional modulation based on time-modulated frequency diverse arrays. IEEE Access, 2017, 5: 26279–26290

39 Ji S, Wang W Q, Chen H, et al. On physical-layer security of FDA communications over Rayleigh fading channels. IEEE Trans Cogn Commun Netw, 2019, 5: 476–490

40 Qiu B, Tao M, Wang L, et al. Multi-beam directional modulation synthesis scheme based on frequency diverse array. IEEE Trans Inform Forensic Secur, 2019, 14: 2593–2606

41 Wang W Q. Retrodirective frequency diverse array focusing for wireless information and power transfer. IEEE J Sel Areas Commun, 2019, 37: 61–73

42 Llombart N, Cooper K B, Dengler R J, et al. Confocal ellipsoidal reflector system for a mechanically scanned active terahertz imager. IEEE Trans Antenn Propagat, 2010, 58: 1834–1841

43 Zhang B, Liu W. Positional modulation design based on multiple phased antenna arrays. IEEE Access, 2019, 7: 33898–33905

44 Lin J, Li Q, Yang J, et al. Physical-layer security for proximal legitimate user and eavesdropper: a frequency diverse

array beamforming approach. IEEE Trans Inform Forensic Secur, 2018, 13: 671–684
45 Chen K, Yang S, Chen Y, et al. Accurate models of time-invariant beampatterns for frequency diverse arrays. IEEE Trans Antenn Propagat, 2019, 67: 3022–3029
46 Xu Y, Shi X, Li W, et al. Low-sidelobe range-angle beamforming with FDA using multiple parameter optimization. IEEE Trans Aerosp Electron Syst, 2019, 55: 2214–2225
47 Xing C, Ma S, Zhou Y. Matrix-monotonic optimization for MIMO systems. IEEE Trans Signal Process, 2015, 63: 334–348
48 Xing C, Zhao X, Xu W, et al. A framework on hybrid MIMO transceiver design based on matrix-monotonic optimization. IEEE Trans Signal Process, 2019, 67: 3531–3546
49 Gong S, Xing C, Chen S, et al. Secure communications for dual-polarized MIMO systems. IEEE Trans Signal Process, 2017, 65: 4177–4192
50 Gong S, Xing C, Chen S, et al. Polarization sensitive array based physical-layer security. IEEE Trans Veh Technol, 2018, 67: 3964–3981
51 Gong S, Xing C, Ma S, et al. Secure wideband beamforming design for two-way MIMO relaying systems. IEEE Trans Veh Technol, 2019, 68: 3472–3486
52 Cui S Q, An J P, Zhang F, et al. Burst frame synchronization in low SNR. In: Proceedings of 2013 International Conference on Mechatronic Sciences, Electric Engineering and Computer (MEC), 2013. 1284–1287
53 Xu H Z, Wei W J, Zhang B, et al. Joint frequency-phase estimation for pilot-limited communication systems: a novel method based on length-variable auto-correlation operator. Sci China Inf Sci, 2019, 62: 169303
54 Liu Y, Ruan H, Wang L, et al. The random frequency diverse array: a new antenna structure for uncoupled direction-range indication in active sensing. IEEE J Sel Top Signal Process, 2017, 11: 295–308
55 Nusenu S Y, Wang W, Ji S. Secure directional modulation using frequency diverse array antenna. In: Proceedings of 2017 IEEE Radar Conference (RadarConf), 2017. 0378–0382
56 Re P D H, Podilchak S K, Constantinides C, et al. An active retrodirective antenna element for circularly polarized wireless power transmission. In: Proceedings of 2016 IEEE Wireless Power Transfer Conference (WPTC), 2016. 1–4
57 Pon C. Retrodirective array using the heterodyne technique. IEEE Trans Antennas Propagat, 1964, 12: 176–180
58 Yao A, Wu W, Fang D. Frequency diverse phase-conjugating retrodirective array with simultaneous range-focusing capability for multi-targets. In: Proceedings of 2015 Asia-Pacific Microwave Conference (APMC), 2015. 1–3
59 Nusenu S Y, Huaizong S. Green secure communication range-angle focusing quadrature spatial modulation using frequency modulated diverse retrodirective array for mmWave wireless communications. IEEE Trans Veh Technol, 2019, 68: 6867–6877
60 Xu Y, Li W, Qin W. The test and evaluation of GPS on-board clock. In: Proceedings of 2013 Joint European Frequency and Time Forum and International Frequency Control Symposium (EFTF/IFC), 2013. 295–298
61 Goldsmith A. Wireless Communications. Cambridge: Cambridge University Press, 2005
62 DiDomenico L D, Rebeiz G M. Digital communications using self-phased arrays. IEEE Trans Microwave Theor Techn, 2001, 49: 677–684
63 Yu J, Cali J, Zhao F, et al. A direct digital synthesis based chirp radar transmitter in 0.13 μm SiGe technology. In: Proceedings of 2013 IEEE Bipolar/BiCMOS Circuits and Technology Meeting (BCTM), 2013. 41–44
64 Kay S M. Fundamentals of Statistical Signal Processing. Upper Saddle River: Prentice Hall PTR, 1993